UMEÅ UNIVERSITY

Fuel conversion and ash formation interactions

A thermochemical study on lignocellulosic biomass

Anna Strandberg

Thermochemical Energy Conversion Laboratory
Department of Applied Physics and Electronics
Umeå 2018

Dissertation for PhD
ISBN: 978-91-7601-871-2
Cover illustration: 3D reconstruction of wheat straw char, by Mikael Tyrel
Electronic version available at: http://umu.diva-portal.org/
Printed by: Service Centre, KBC, Umeå University
Umeå, Sweden, 2018

“Learn from yesterday, live for today, hope for tomorrow. The important thing is not to stop questioning” - Albert Einstein

Table of Contents

Abstract ... ii
Sammanfattning på svenska ... iii
Appended publications ... v
Author's contributions ... vi
Other scientific publications ... vii
1 Introduction ... 1
1.1 Objective ... 3
2 Thermochemical conversion of lignocellulosic biomass ... 5
2.1.1 Ash-forming matter in lignocellulosic biomass ... 6
2.1.2 Pretreatment ... 6
2.2 Fuel conversion ... 7
2.2.1 Torrefaction ... 8
2.2.2 Devolatilization ... 8
2.2.3 Char conversion ... 9
2.2.4 Ash formation ... 11
3 Materials and Methods ... 16
3.1 Fuels and fuel analysis ... 16
3.2 Experimental setups ... 16
3.2.1 Drop-tube furnace ... 17
3.2.2 Laboratory scale single pellet furnace ... 18
3.2.3 Domestic pellet boiler ... 19
3.3 Analytical methods ... 20
3.3.1 Thermogravimetric analyzer ... 21
3.3.2 Scanning Electron Microscopy ... 22
3.3.3 X-ray micro-tomography and image analysis ... 23
3.3.4 Powder X-ray diffraction ... 25
3.4 Data analysis ... 27
3.4.1 Multivariate data analysis ... 27
3.4.2 Thermodynamic equilibrium calculations ... 28
3.4.3 Viscosity estimation ... 29
4 Results and discussion ... 30
4.1 Fuel devolatilization and char morphology ... 30
4.1.1 Char conversion rate ... 35
4.2 Ash formation ... 37
4.2.1 Si-rich silicate forming fuels ... 37
4.2.2 Ca-rich carbonate and oxide forming fuels ... 43
5 Conclusions ... 50
6 Future work ... 53
Acknowledgement ... 54
References ... 56

Abstract

Biomass is considered to be CO_2 neutral, and to be able to reduce the dependency on fossil fuels the need for expanded and sustainable biomass feedstock is increasing. Ash-related problems are some of the most important aspects of this increasing use of new biomass assortments in thermal energy conversion systems. An improved basic understanding of fuel conversion, ash formation, ash transformation and ash interactions with the converting fuel is therefore important.

In the present thesis, the main objective was to provide new knowledge on thermochemical fuel conversion, specifically on how ash formation interacts with fuel conversion for lignocellulosic biomasses. The main methods used were experimental characterization of decomposition behavior and analysis of morphology and elemental composition of samples, using different appliances, analytical methods and fuels. Multivariate data analysis was successfully used on thermogravimetric data for prediction of compositional data and fuel properties.

New, detailed explanations of structural changes in char morphology and ash properties during conversion were provided including descriptions of the influences of ash formation on fuel conversion rates under different conditions. The influences were found different depending on both particle size and ash composition. One implication of these findings is that for fuels with low temperature melting ash, the diffusion barrier formed causes difficulties for typical thermogravimetric experiments aiming at determination of reactivity in the kinetically controlled regime. This is recommended to carefully consider for future studies. On a single pellet level, char encapsulation was not found to dominate and limit gas transport and conversion for any of the fuels tested. In practical applications, however, the situation may be different with thick ash layers accumulating on a fuel bed surface. Another important finding was the extensive formation of cracks and internal cavities during combustion of pellets, providing new insights in the fundamentals of fuel conversion.

Clean woody fuels, rich in calcium, formed a porous ash layer with no sign of limiting char conversion rates. The phase chemical transformations involving carbonate and oxide formation from poplar pellets was studied in detail. For grassy fuels, on the other hand, low melting point silicates are expected to form. The physical properties of K-Ca-silicates from silicon rich straw fuels were also characterized, providing new insights on ash formation on micrometer scale resolution; at high temperature, the silicate melt formed bubbles on the surface that partially covered the char, while for lower temperature a more rigid net structure was formed.

Sammanfattning på svenska

Ett ökat intresse för att nyttja nya biomassabaserade råvarufraktioner som bränslen i olika processer drivs av den pågående omställningen av energisystemen med målet att minska beroendet av fossila bränslen. ”Nya” biobränslen inbegriper ofta snabbväxande grödor, tidigare outnyttjade växtdelar eller industriella restprodukter som på grund av dålig lönsamhet eller tekniska problem varit svåra att omvandla till nyttig energi. Problemen associerade till dessa bränslen är ofta relaterade till innehållet av näringsämnen och mineraler, av vilka många i processen blir de askbildande elementen. Biomassa är en mycket blandad grupp av bränslen vilket innebär en stor variation av mängden och sammansättningen av de askbildande elementen, både mellan bränslen och mellan olika delar av samma bränsle.

Det är välkänt att de askbildande elementen i biobränslen kan vara problematiska i förbränningsanläggningar, med beläggningsbildning, korrosion och slaggning, det vill säga när smält aska bildar en sintrad ask-kaka som kan vara svår att avlägsna. Något som är desto mindre känt är hur askföreningar påverkar själva utbränningsförloppet för en bränslepartikel. Tidigare forskning har visat att vissa askelement kan påskynda processen. Erfarenheter visar också att höga halter av vissa askbildande element kan bilda fysikaliska barriärer på partikelytan som kan inhibera processen, främst avseende koksomvandling. Hastigheten för partikelomvandling är viktig i många processer och i vissa fall avgörande för framgång. Dessa frågor utgör bakgrunden till denna avhandling.

I denna avhandling var målet att generera ny kunskap om bränsleomvandling (förgasning och förbränning) och askbildning, samt att ge ny information om hur askbildningen interagerar med bränsleomvandling för lignocellulosisk biomassa. Primärt fokus har varit på den så kallade koksomvandlingen och askbildningen under koksomvandlingen.

Denna studie ger nya, tidsupplösta och omvandlingsbaserade förklaringar av detaljerade strukturella förändringar av bränslets sammansättning, morfologi och askbildning vid termisk omvandling av lignocellulosisk biomassa. Hastigheten för koksomvandlingen påverkades både av partikelstorlek och av askans sammansättning. Resultatet i detta arbete pekar på att bränslen med låg asksmältningstemperatur kan, även för mycket tunt lager av fint pulver, bilda en diffusionsbarriär på grund av smält aska, vilket kan förhindra att reaktionen sker till fullo i den kinetiskt styrda regimen. I framtida kinetikstudier rekommenderas därför att hänsyn tas till dessa aspekter. Denna totala inkapsling av eventuell kvarvarande koks, med begränsning på gastransport och bränsleomvandling, hittades inte på enpelletsnivå. I praktiska tillämpningar i större skala, kan

situationen emellertid vara annorlunda eftersom tjockare askskikt ackumuleras på en bränslebädd.

Istället för ovan nämnda täckande asklager bildade vetehalmen bubblor av smält silikatrik aska på ytan vid förbränning på enpelletsnivå vid hög temperatur. Dessa bubblor täckte bara delar av ytan. Vid lägre temperatur bildades istället en annan struktur på den silikatrika askan, mer format som en stabil nätstruktur med lägre andel smälta.

Träbaserade bränslen, med hög halt av kalcium, bildade ett poröst asklager, utan tecken på att begränsa omvandlingshastigheten. Vid lägre temperatur bildar askan huvudsakligen karbonater; denna fraktion minskar när temperaturen ökar och vid hög temperatur domineras sammansättningen i stället av oxider. Detta är väl känt sedan tidigare, men fasomvandlingarna i en brinnande pellet kopplat till de lokala förhållandena i densamma visades för första gången i denna avhandling. I denna avhandling presenteras också viktiga resultat framtagna med hjälp av röntgenbaserad mikrotomografi för 3D avbildning och analys av mikrostrukturer. Vi kunde konstatera att det bildades stora mängder sprickor och inre håligheter i pellets under förbränning vid hög temperatur, vilket ger nya pusselbitar till den fundamentala förståelsen av bränslepartikelomvandling.

Appended publications

This thesis includes the following publications, referred to in the text according to their roman numbers.

I. A. Strandberg, P. Holmgren, M. Broström, Predicting fuel properties of biomass using thermogravimetry and multivariate data analysis, *Fuel Processing Technology*, 156 (2017) 107-112.

II. A. Strandberg, P. Holmgren, D.R. Wagner, R. Molinder, H. Wiinikka, K. Umeki, M. Broström, Effects of Pyrolysis Conditions and Ash Formation on Gasification Rates of Biomass Char, *Energy & Fuels*, 31 (2017) 6507-6514.

III. A. Strandberg, M. Thyrel, N. Skoglund, T.A. Lestander, M. Broström, R. Backman, Biomass pellet combustion: Cavities and ash formation characterized by synchrotron X-ray micro-tomography, *Fuel Processing Technology*, 176 (2018) 211-220.

IV. A. Strandberg, M. Thyrel, N. Skoglund, T. A. Lestander, M. Broström, R. Backman, Time-dependent studies of silicate slag formation during combustion of wheat straw. *Manuscript*.

V. A. Strandberg, M. Carlborg, C Boman, M. Broström, Ash formation and transformation during combustion of poplar wood pellets. *Manuscript*.

Author's contributions

Paper I. Predicting fuel properties of biomass using thermogravimetry and multivariate data analysis

Strandberg contributed to planning the work. Strandberg performed the experimental work. Strandberg carried out the multivariate data analysis and contributed to the analysis and discussions of the findings. Strandberg wrote the majority of the paper.

Paper II. Effects of pyrolysis conditions and ash formation on gasification rates of biomass char

Strandberg contributed to planning the work. Strandberg performed the drop-tube experiments together with Holmgren and Wagner. Strandberg carried out the TGA experiments, performed the analysis, and wrote the majority of the paper.

Paper III. Biomass pellet combustion: Cavities and ash formation characterized by synchrotron X-ray micro-tomography

Strandberg contributed to planning the work. Strandberg performed the combustion experiments. All authors contributed to the micro-tomography experiments at ALS. Strandberg carried out the SEM-EDS analysis, contributed to evaluation of the results and wrote the majority of the paper.

Paper IV. Time-dependent studies of silicate slag formation during combustion of wheat straw

Strandberg contributed to planning the work. Strandberg performed the single pellet combustion experiments. Strandberg contributed to the micro-tomography experiments at ALS. Strandberg carried out the SEM-EDS analysis, contributed to evaluation of the results, and wrote the majority of the paper.

Paper V. Ash formation and transformation during combustion of poplar wood pellets

Strandberg contributed to planning the work. Strandberg performed the single pellet combustion experiments. Strandberg carried out the SEM-EDS analysis, participated in the XRD analysis, contributed to evaluation of the results, and wrote the majority of the paper.

Other scientific publications

Additional publications of relevance although not included in the thesis.

Peer-review papers

1. P. Holmgren, D.R. Wagner, A. Strandberg, R. Molinder, H. Wiinikka, K. Umeki, M. Broström, Size, shape, and density changes of biomass particles during rapid devolatilization, *Fuel*, 206 (2017) 342-351.

Conference proceedings

1. A. Persson*, P. Holmgren, M. Broström, Decomposition modelling using thermogravimetry with a multivariate approach, in: 21nd European Biomass Conference and Exhibition, Copenhagen, June, 2013, ETA Florens Renewable Energies, 2013.
2. A. Strandberg, D.R. Wagner, P. Holmgren, R. Molinder, H. Wiinikka, K. Umeki, M. Broström, Influence of Biomass Particle Properties and Pyrolysis Conditions on Char Reactivity, in: Impacts of Fuel Quality on Power Production October 26–31, 2014 Snowbird Resort & Conference Center Snowbird, Utah, 2014.
3. P. Holmgren, A. Strandberg, D.R. Wagner, R. Molinder, H. Wiinikka, K. Umeki, M. Broström, Size, Shape and Density Changes of Biomass Particles during Devolatilization in a Drop Tube Furnace, in: Impacts of Fuel Quality on Power Production October 26–31, 2014 Snowbird Resort & Conference Center Snowbird, Utah, 2014.
4. D.R. Wagner, P. Holmgren, A. Strandberg, H. Wiinikka, R. Molinder, M. Broström, Fate of Inorganic Species during Biomass Devolatilization in a Drop Tube Furnace, in: Impacts of Fuel Quality on Power Production October 26–31, 2014 Snowbird Resort & Conference Center Snowbird, Utah, 2014.
5. A. Strandberg, M. Thyrel, M. Rudolfsson, T.A. Lestander, R. Backman, N. Skoglund, M. Broström, Char conversion characterized by synchrotron based X-ray micro-tomograhy and SEM-EDS analysis, in: The 25th European Biomass Conference and Exhibition, 2017.

The conference proceedings (1-2) were later revised and published as papers I-II, and conference proceeding 5 was revised and published as paper III.

* Persson was the author's maiden name.

1 Introduction

Combustion of solid fuels is one of mankind's oldest technologies, and still plays an important role in our society. Thermal conversion processes provide almost 90% of the energy used today for electrical power generation, heating, and transport. The total energy production in the world is increasing, and there is a corresponding increase in greenhouse gas emissions [1]. Climate researchers state that the human impact on the climate system is clear (United Nations' Intergovernmental Panel on Climate Change (IPCC), 2013 [2]) and that the use of energy is the largest contributor of emissions among the many human activities that produce greenhouse gases. Today, 82% of the world's total primary energy supply relies on fossil fuels (2015) [1]. Coal is responsible for 45% of the global CO_2 emissions, even though it only contributes 28% of the total primary energy supply, due to its high carbon content per unit of energy released [1]. The use of fossil fuels must be decreased to meet environmental and sustainability challenges such as climate change, population growth, increasing global energy demand, etc. In studies on planetary boundaries by Rockström et al. [3], and Steffen et al. [4], climate change is identified as one of two core boundaries together with biosphere integrity because of their fundamental importance for the Earth system; each of these has the potential on their own to drive the Earth system into a new state.

In December 2015, most of the world leaders and nations were united in The Paris Agreement, United Nations Framework Convention on Climate Change [5], which brings all nations together in a common cause to take action to reduce greenhouse gas emissions, to combat climate change and adapt to its effects, and to provide enhanced support to assist developing countries in doing so. Biomass is an important energy source today, which is both renewable and CO_2 neutral. Supplemented with other renewable energy technologies (solar power, wind power, hydropower, geothermal heat, etc.) and increased energy conservation and efficiencies, it can be used to reduce the dependence on fossil fuels and help to achieve the climate goals.

Biomass is the primary energy supply in many developing countries; firewood is the primary fuel for cooking and heating. In these developing countries, biomass accounts for 35% of primary energy consumption and world-wide biomass provides about 14% of the world's primary energy consumption [6]. In modern usage, the biomass is converted into high-quality energy carriers, such as electricity, combined heat and power, and biomass liquid fuels for transport, but the biomass can also be converted to "green chemicals" and new bio-based materials. The use of biomass has potential to grow, and the need for more feedstock will therefore probably increase.

Woody biomass has for many years been considered one of the most important biomass resource for bioenergy production. However, the availability of these raw materials is limited in many areas, and wood is also considered a material for higher value products [7]. To meet the increase in biomass utilization, alternative fuel assortments are being introduced to the market. Increased use of biomass sources from natural ecosystems may lead to serious environmental problems. Therefore, there is a need for an increased use of more "new" types of biomasses such as short rotation energy crops, agricultural crops and residual products, from both forestry and agricultural origin. However, the sustainability of the biomass must be considered, and issues such as competition with food production on fertile land and water resources, loss of forests and biodiversity, and net greenhouse gas emissions through land-use change must be addressed [8]. These issues can be taken into account by using forest and agricultural residues (non-edible), contaminated biomass and industrial biomass wastes, and short-rotation energy crops (grass, forest and algae plantations), but grown only on existing low productive, degraded or contaminated land not suitable for farming, or in wastewater or contaminated ponds [9]. In a study by Hoogwijk et al. [10], six biomass resource categories for energy were identified (energy crops on surplus cropland, energy crops on degraded land, agricultural residues, forest residues, animal manure and organic wastes) and the range of the global potential of primary biomass (in about 50 years) was very broad, quantified to 33–1135 EJ y^{-1}. Another example is residues from production of agricultural crops that have been estimated to correspond globally to about 6700 Tg y^{-1} [11]. Yet today, especially in developing countries, the surplus crop residues are burned in the open air, causing both energy loss and air pollution.

These "new" broad biomass assortments varies widely in composition. From a fuel perspective, the amount and composition of ash-forming elements in particular varies greatly between fuels, and it can also be heterogeneous in the same fuel [12-15] resulting in differing ash composition and amount of ash in combustion processes [16]. Some of the most important aspects of increased utilization of biomass and new biomass assortments in thermal energy conversion systems are connected to ash-related operational problems, which often limit fuel flexibility at existing power plants and generating high investments costs when building new ones. It is well known that the ash element in biomass fuels, with differing ash content and ash compositions can be problematic in furnaces, with deposit formation, corrosion, aerosol formation, and in some cases unfavorable ash-melting temperatures, which can lead to problems with slagging and resultant problems in the ash removal system [17-19]. On the other hand, some of these ash-forming elements can have a positive impact on the process and, for example, can reduce slagging tendencies or act as catalysts during thermal conversion [20-22].

Many important parameters on a large-scale reactor level, such as decomposition behavior, overall fuel conversion rate and ash formation, are highly dependent on the processes involved in the conversion of individual biomass particles. Full-scale experiments are both expensive and pose a large logistic challenge. It is also very difficult, and sometimes almost impossible, to control and measure all relevant parameters. Research using experiments on a laboratory scale and pilot-scale equipment can increase our fundamental knowledge. Modelling of conversion processing can provide a method to transfer subscale experiments to large-scale applications. Modelling and simulation of thermal conversion processes also provide a better understanding of how physical and chemical properties of the fuel influence the overall performance of boilers. Optimized reactor design and operational conditions contribute to obviating expensive trial and error. Many studies have focused on modelling devolatilization and oxidation of larger, thermally thick biomass particles [23-31], but only a limited number of papers describe specifically conversion of densified biomass particles, e.g. pellets [32-34]. Furthermore, numerical conversion models often either disregard [24, 27] or simplify [23, 26] the formation of an ash layer, its physical properties, chemical composition, and its effects on fuel conversion. Only in a few studies is ash formation partially implemented in fuel conversion models [30, 35-37]. However, the potential for a robust predicting or modelling system would increase with more detailed knowledge on the chemical conversion characteristics for different types of fuels and to increase the understanding of how the ash-forming matter reacts during thermal conversion processes.

1.1 Objective

The main objective of the present thesis was to provide new knowledge on thermochemical fuel conversion for different types of lignocellulosic biomasses, and to describe how ash formation interacts with fuel conversion. Specific objectives for the respective paper were to:

Paper I: Evaluate and demonstrate the potential for using a multivariate statistical approach on thermogravimetric data for determining fuel properties of wood, with focus on the degree of decomposition of thermally treated wood, and to compare the predictions from the multivariate model with a conventional curve deconvolution approach made to the same dataset. Finally, to test the approach for predictions of other properties, such as elemental composition, heating value and content of volatiles.

Paper II: Evaluate intrinsic gasification rates of chars generated from rapid devolatilization of biomass particles of different sizes, to study if and how char reactivity changes depend on the parameters varied. Two different fuels were included to represent both woody and agricultural biomass: wood from Scots pine

and straw from wheat. The second objective of this study was to compare gasification profiles of chars from the two fuels, and to further develop the theories of fuel-ash interactions using compositional data together with observations on reactivity profiles and ash formation during gasification.

Paper III: Provide new detailed information on char morphology and the development of cracks and cavities and ash layers in relation to time and char conversion during pellet combustion at a single pellet level. The aim was also to provide 3D density data that describes the development of cracks and internal cavities in the char during conversion, as well as density data for the formation of ash by analyzing the chars with synchrotron-based X-ray micro-tomography. For this study, two different biomass pellets with very different composition of a mainly inorganic fraction were used: poplar wood and wheat straw.

Paper IV: Provide more detailed descriptions of transport and reactions of ash-forming elements in wheat straw pellets during combustion at different temperatures and in relation to time and char conversion. The description stretches beyond the conclusions that can be drawn from pure inorganic reactions at equilibrium since availability and reaction rates are affected by the presence of the converting char and the temperature distribution in the pellet is higher than that of the surroundings due to the reaction heat.

Paper V: Perform a detailed characterization of the ash formation and transformation at a single-pellet level during combustion of a poplar fuel. Combustion tests were performed using poplar pellets in a single-pellet isothermal thermogravimetric analyzer operated at different temperatures and atmospheres, and the quench cooled char and residual ashes were characterized for morphology and chemistry (elemental distribution and phases). In addition, thermodynamic equilibrium calculations were used both to plan the experiments and to support the interpretation of experimental results.

2 Thermochemical conversion of lignocellulosic biomass

Biomass can be defined as a natural constituent that are constantly replenished and can be derived directly or indirectly from plant photosynthesis, generated via animal and human food digestion, or as technogenic products derived via processing of the above mentioned natural constituent [13]. Roughly, biomass can be divided into groups according to biological diversity and source: wood and woody biomass; herbaceous and agricultural biomass; aquatic biomass; animal and human biomass waste; contaminated biomass and industrial biomass wastes; and biomass mixtures (blends of the other groups) [13]. In the present thesis, the focus is on lignocellulosic biomass, which is plant or plant-based material, such as wood and woody biomass and herbaceous and agricultural biomass.

All types of lignocellulosic biomasses are mainly composed of cellulose, hemicellulose and lignin; these are the structural components. Cellulose is well defined and is composed of chains of D-glucose units linked by β-(1→4) glycosidic bonds [38]. Hemicellulose is a heterogeneous group of structurally diverse polysaccharides, the most important biological role of which is to strengthen the cell wall by interaction with cellulose and, in some walls, with lignin [39]. The hemicellulosic fraction differs significantly in different types of plants and in different cell types within plants, both in relative abundance and composition [39]. The decomposition behavior varies significantly between different hemicelluloses [40], but overall it is less thermally stable than cellulose. Lignin is a complex and highly variable phenolic polymer, it acts as “glue” keeping the fiber cells together, which is important for mechanical support, and it is also important for water and nutrient transport [41]. In addition, the insolubility and complexity of the lignin polymer has an important function in plant defense by resisting degradation by microorganisms [41].

There are also smaller but varying amounts of extractives and inorganic ash-forming elements present in the plant material. The proportions of the components and the composition of the ash-forming elements can both vary depending on e.g. the type of plant, the part of the plant, age of the plant, growth location, soil condition, fertilizer, harvesting technique, time of harvesting, and contaminations [11, 13, 14, 42, 43].

2.1.1 Ash-forming matter in lignocellulosic biomass

Most of the inorganic elements present in lignocellulosic biomass act as nutrients and have important biological functions. The diversity has been characterized and extensively discussed in previous studies [12-15, 20, 44-46]. The most important ash-forming elements in lignocellulosic biomass can be limited to Si, Ca, Mg, K, Na, P, S, Cl, Al, Fe, and Mn [21]. The ash yield is normally lower for wood and woody biomass, which is commonly enriched in calcium and potassium, than for herbaceous and agricultural biomass, the composition of which varies largely, but is normally dominated by silicon, potassium, calcium, and also enriched in chlorine and phosphorus as well as sulfur [13, 46]. The differences might depend on the fact that the herbaceous and agricultural biomass group has a different organic structure, a more rapid metabolism, and therefore takes up more nutrients during the growing periods [13, 47].

The ash-forming elements in lignocellulosic biomass are present in various chemical forms, i.e. as organically bound ash-forming elements, as dissolved salts (soluble ions), or as minerals [46, 48, 49]. The minerals can, to a varying degree, be incorporated in the fuel structure, or as extraneous material from impurities and contaminations during growing or handling. E.g. sand contaminants can be recognized as substantial amounts of silicon and aluminum in the fuel [46]. The behavior of the ash-forming matter during conversion can depend on the form in which it is present in the fuel, and might depend on whether its origin is biological or non-biological [46, 48]. Extraneous material, for example sand (mainly quartz and feldspar), clay minerals and carbonates are generally less reactive than the inherent biomass ash-forming matter [21], and biologically originating potassium has shown to exhibit far higher mobility than non-biological which is present as soil contaminants and additives to the fuels [18].

2.1.2 Pretreatment

Biomass sometimes has impractical physical properties, with for example a low bulk density and varying moisture content. Biomass storage, transportation and handling are costly since many raw materials have very low bulk densities, (for example sawdust, grass, straw). Various pretreatments of biomass are performed in order to obtain more favorable fuel properties. Physical pretreatment includes size reduction and drying, but also densification, i.e. production of briquettes or pellets [50, 51]. Biomass wood pellets are widely used for heat and power production, for both domestic heating and for large-scale district heating or co-firing, and over the past 10 years the global production of wood pellets has increased steadily surpassing 26 Mt in 2015 [52].

Both raw material and pelletizing conditions, for example moisture content, particle size distribution, pelletizing temperature and pressure affect the physical

properties of the pellets, such as density, conductivity, permeability, pore structure and durability [50, 53-55]. Pellet properties in turn can affect conversion behavior, for example the time of devolatilization and char conversion, shrinkage or swelling, and particle temperature [56, 57].

2.2 Fuel conversion

Thermochemical conversion processes involve heat in the conversion of the fuel to other chemical forms, and are a result of interaction between the heat, mass transport phenomena and chemical reactions. The main processes are combustion (generating heat and electricity), and pyrolysis and gasification (mainly for production of liquid and gaseous fuels or other chemicals, or for efficient heat and power generation) [22]. Pyrolysis, or devolatilization, is also an important first chemical step during gasification and combustion.

Generally, fuel conversion can be described as different overlapping and interacting steps, from the solid fuel to solid residues, aerosols and gases. Figure 1 presents the thermal conversion of a fuel particle, illustrated using images of poplar pellets from different steps of interrupted combustion tests. When a biomass particle is placed in a hot environment it will be heated and dried; devolatilization (pyrolysis) converts the fuel into gas (including some reactive ash-forming elements) and a solid carbon rich char particle. After the volatile species have left the char particle, char oxidation (char conversion) converts char by reacting with oxygen, or carbon monoxide and water vapor (gasification). The solid residue after complete oxidation of the char is the residual ash (bottom ash). These steps occur simultaneously in the fuel bed of a real furnace with continuous feeding.

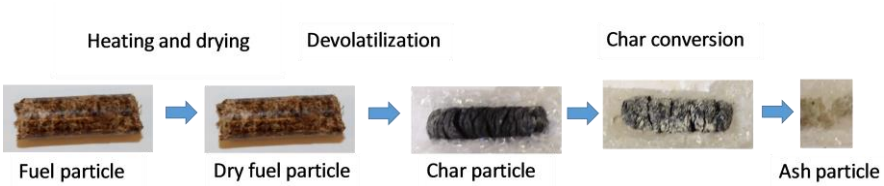

Figure 1. Images of poplar pellet from different steps of thermal conversion.

2.2.1 Torrefaction

Thermal and thermochemical pretreatment can be used to improve some physical and chemical fuel properties, for example to increase the energy density. Different process concepts, i.e. torrefaction, steam explosion, hydrothermal carbonization and low temperature pyrolysis, work in different conditions such as different temperatures, gas environment, steam addition, residence time and pressure. In the present thesis, the fundamental fuel decomposition behavior was studied under conditions resembling the torrefaction process.

Torrefaction is a thermal pretreatment method operated in an inert or low oxygen atmosphere in a temperature range of 200-350°C and at atmospheric pressure [58]. The biomass is partly decomposed during torrefaction, mainly by decomposition of hemicellulose, and the amount of bound oxygen and hydrogen decreases, with resultant lower O/C and H/C ratios and thereby increased calorific value on a mass basis [59-61]. Different conditions during the process (temperature, inert gas, reaction time) and biomass resources result in variations in solid, liquid and gaseous products.

Important advantages of torrefaction are improvement in energy density, increased heating value, and less hydrophilic biomass (decreased moisture uptake) [60-62]. An improvement in grindability characteristics, with less fibrous material after milling and decreased milling energy, was observed when comparing torrefied with raw biomass [59, 61, 63].

2.2.2 Devolatilization

After drying, the heated particle starts to decompose. Overall, this process is endothermic and thus requires energy, even though some of the devolatilization reactions are exothermic. The outgoing volatiles block the inward oxygen transport (if an oxidizing agent is present), meaning the particle will undergo devolatilization under a locally inert atmosphere. Fuel devolatilization involves great complexity in which both transport phenomena and chemical reactions are important, as well as interactions between them [64]. The terms devolatilization and pyrolysis are often confused. In the present thesis, pyrolysis refers to a process without access to an oxidizing agent, while devolatilization refers to the phenomenon when the fuel decomposes into volatile product and char.

Normally the devolatilization products are divided into gas, tar and char. Depending on the heating rate, the reactor temperature and pressure, and the size and composition of the fuel, the yield and properties of the products can vary significantly [22, 65-70]. Particle size influences the mass and heat transfer, and to some extent also the internal secondary reactions in the particles. Because of thermal inertia, larger particles have a larger temperature gradient and thus

slower efficient heating rates in high heating rate environments [65, 71, 72]. Based on the connected effects of particle size and external heating conditions, three main regimes of solid fuel pyrolysis have been identified and defined with respect to particle size: the thermally thick, the thermally thin, and the purely kinetic regime [73-75].

Both convection and radiation contribute to heat transfer to the particle surface when a biomass particle is inserted in a hot reactor. Inside the particle, heat transfer is dominated by conduction [65]. When the temperature inside the particle increases, moisture vaporization occurs first and then devolatilization starts. During devolatilization, heating of the particle is affected by heat from the chemical reactions and the migration of gaseous products through the porous medium. The devolatilization products result from both primary decomposition of the solid fuel and from secondary reactions of volatile condensable organic products that can occur when volatile products pass the outer reacted region of the fuel particle at high temperature and through the reaction environment. The secondary reactions change the final products of devolatilization to low-molecular weight gases and char [65, 66].

During devolatilization, the particle can undergo shrinkage or swelling, shape change, and morphological changes depending on the heating rate, temperature, pressure, residence time and the composition of the fuel [69, 76, 77]. Stresses due to shrinkage, pressure build-up from volatiles, together with temperature gradients in a particle can result in formation of cracks and, in some cases, fragmentation [78].

2.2.3 Char conversion

Solid residues after devolatilization are called char and consist mainly of carbon and ash with minor amounts of hydrogen and oxygen. After devolatilization, the oxidant can reach the particle, diffuse toward the particle center, and oxidize the char. The devolatilization step is rapid whereas char oxidation is slow, and therefore char oxidation reactions can be considered as rate limiting in most processes [22, 79, 80].

Char conversion processes take place in either a combustion (excess O_2) or gasification (reducing sub-stoichiometric atmosphere) regime. Char combustion, which is strongly exothermic, occurs mostly on the surface of the char or inside large pores, forming primarily CO and CO_2 [81]. In addition, inorganic material is released; this is discussed further in 2.2.4. The gases formed from char combustion move away from the char particle and can react further with gases formed during volatilization. Hence, the CO/CO_2 equilibrium can for example shift to different distances from the fuel particle. CO_2 and H_2O are the main and

desired products from complete combustion, while incomplete combustion can also result in the formation of carbon monoxide, volatile hydrocarbons, polycyclic hydrocarbons and soot, which can be both particulate and gaseous [81]. During oxidation, the temperature gradient inside the particle can vary. Char oxidation of large particles is highly influenced by a combination of chemical kinetics, mass transfer, heat transfer and heat of reactions [82, 83].

Gasification is conversion of carbonaceous fuel to a product gas with a useable heating value. The process can be described as partial oxidation, often achieved using a controlled supply of air, O_2, CO_2 and/or H_2O, producing a synthesis gas [84]. The synthesis gas mainly consists of the combustible components H_2, CO, CO_4 in varying ratios, but also H_2O and CO_2, and generally unwanted soot and tar compounds. The content depends on the feedstock, oxidizing agent and the process conditions, such as temperature and pressure [84]. Gasification can be divided into four steps; in addition to the previously mentioned heating, drying and devolatilization, they include gas-solid reactions and gas phase reactions, both oxidation and reduction [81].

Char conversion rate

Among others, reviews by Laurendeau [85], Hurt [86] and Di Blasi [22] provide an overview of combustion and gasification rates of chars. Highly simplified, char conversion rates are determined by a combination of chemical kinetics and transport processes in and around the fuel particle, including the mass transfer of reaction agents inside the pore structure of char, mass transfer of reaction agents through the external boundary of the particle or film diffusion, and diffusion through the ash layer. Depending on which of the above-mentioned processes dominate, control of the overall reaction rate, the char conversion, can be divided into three conversion regimes [87, 88]. In regime I, heat and mass transfer limitations are avoided, and chemical reaction kinetics limit the reaction rate. In regime II, both the transport process with pore diffusion and chemical reactions are important in determining the mass loss rate. In regime III, rates are limited by boundary-layer diffusion. Many theoretical models are built on the classic theory of Thiele [89] describe heterogeneous reaction and diffusion in porous media.

The intrinsic kinetics rates are defined as those rates that are not influenced by transport processes (regime I). To evaluate the intrinsic kinetics, small particle size and low mass, relatively low temperature and good mixing with gaseous reagents are needed [7, 90-93]. For thermogravimetric measurements, the crucible location also needs to be taken into consideration for accurate interpretation of diffusion effects [22]. At high temperature, and for larger particle sizes, regime II and III conditions are predominant, and particle density and size are important parameters [86].

Conditions during devolatilization highly affect the char yield and the reactivity during subsequent char conversion (combustion and gasification); high heating rates during devolatilization have been shown to increase the char reactivity for both oxidation and gasification [22, 69, 70], while high temperature and prolonged retention time generally reduce the reactivity of char particles [22, 67, 68, 70]. Chars produced from smaller particles have been associated with higher reactivities, probably connected to intra-particle transport and secondary transformation of products during devolatilization [70, 94].

In addition to pyrolysis conditions, the change in char structure, the distribution of active size, and the ash-forming elements present in the fuel are also known to play important roles in reactivity and char burnout [22, 69]. The effect of the ash-forming elements will be discussed further in 2.2.4.

2.2.4 Ash formation

During thermochemical conversion, the organic structure of the biomass is decomposed, while the inorganic material is either released to the gas in form of condensable vapor species (forming deposits or fly ash), entrained as solid particles (coarse fly ash), or retained as a solid residue (bottom ash) [95]. The outcome depends on the composition and relationship between various elements, the total content of ash, and the process conditions.

Ash formation and transformation reactions are complex and occur through interactions involving many components and the environment, as confirmed by numerous earlier published studies [21, 96, 97]. This can be understood and described in a number of ways; one quite common way is to consider ash components as, at least mostly, oxidic and divide them into basic and acidic compounds. There is a chemical attraction between these categories, and they react with each other in an order according to the reactivity of the compound, easily described by thermodynamic equilibrium calculations [21]. This order has a temperature dependence according to Gibbs free energy, and can be used as a tool to acquire an increased understanding of the complex ash transformation reactions.

The ash transformation reactions were described by Boström et al. [21] by dividing them into primary and secondary reactions, with the starting point as the concentrations of the ash-forming elements, fundamental chemical thermodynamics and knowledge of high-temperature inorganic chemistry. The primary ash transformation reactions are oxidation of the ash-forming elements to the basic and acidic compounds described above. These reactions can be viewed as a basis for the secondary ash transformation reactions. This concept was discussed further in the thesis of Skoglund [98], which also introduced the

concept that oxides and compounds can be ordered according to their relative Lewis base (e-donor) and Lewis acid (e-acceptor) behavior. The Lewis Base/Acid concept basically describes how a chemical system strives to achieve the most stable products under specified conditions, and secondary ash transformation reactions were suggested from the Lewis acids and bases formed from the elements in the fuel [98]. In addition, tertiary ash transformation reactions were defined. The models formulated all aim at predicting ash formation and transformation based on composition and process variables. For example, the fractionation seen in Figure 2 can be determined based on this kind of analysis. The schematic fractionation of the main ash-forming elements during combustion, illustrated in Figure 2 below (Fe, Mn, Na, Al are excluded due to their typically lower concentrations), is based on information on the fuel composition, and in the second box are described as oxides (even though that is not necessarily the final most stable form). The table is constructed in order of descending reactivity, highlighting the thermodynamic stability with preferred reactions between the compounds at the top of the list, in agreement with the description in [21]. Products of primary, secondary or even tertiary reactions, some of them volatile and some refractory, will determine the overall ash formation behavior. Besides composition, temperature is another important parameter; at lower temperature, for example, sulfates and carbonates can stay in the bottom ash.

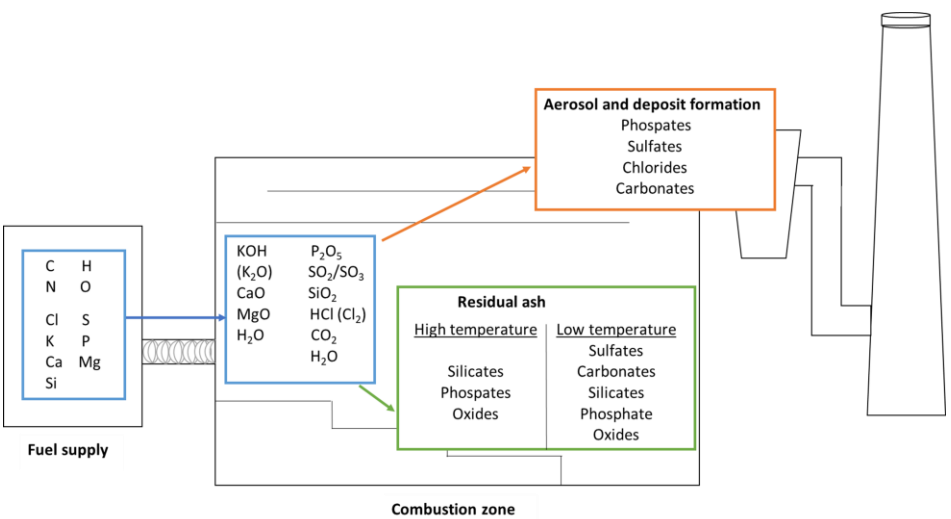

Figure 2. Schematic description of the fractionation of the main ash-forming elements during combustion. To the left, fuel composition; in the middle the main ash-forming components given as oxides; the upper box shows volatilized compounds forming deposits and aerosols; and the box to the lower right presents the bottom/residual ash.

Alkali components play a major role in deposit formation, slagging and bed agglomeration in fluidized bed combustion and gasification. In an alkali-rich fuel, the amounts and type of alkali compounds formed are dependent on the combustion temperature and the presence of other components. Several compounds of phosphorus, chlorine and sulfur have a high initial volatility, and these elements could evaporate to a large extent if no further interaction with other ash elements takes place to form more stable condensed phases [21]. K-phosphate and K-chloride have low melting points and their volatilization increase with temperature. If CaO and MgO are available, non-volatile mixed compounds of K – Ca - and K – Mg – phosphates can be formed [21]. These compounds will remain in the residual ash. Otherwise, some K-phosphate will probably evaporate and leave the fuel. Chlorine evaporates to the flue gas, often in the form of HCl at low temperature, or as KCl mainly between 700 and 800°C [99, 100]. A simplified description of the balance between retention and volatilization is the use of indices, e.g. K/Si and Cl/K molar ratios, which have a significant effect on potassium release or retention in the residual ash [19, 97, 99, 100]. However, they do not take in account the full complexity of the ash reactions, and even though useful in some cases, they cannot be generalized without including more elements and conditions. Increased predictability has been shown by others by covering more fuel scenarios and possible reaction paths [96, 101, 102].

A significant part of the fuel sulfur can be released to the gas phase already at 500°C [100]. Previous investigations indicate that organically bound sulfur is more likely to be released to the gas phase at low temperatures than other forms of sulfur, due to lower thermal stability [103, 104]. Additional sulfur might gradually be released to the gas phase above 700°C. Notwithstanding, the retention of sulfur in the ash is dependent on the fate of calcium and potassium during burnout, and silicates were found to enhance sulfur volatilization by competing reactions with calcium and potassium [104]; fuels with low silicon content had 20-50% S retained in the ash, while for combustion of straw 85% of the S was released at 950°C [100, 104]. For example K_2SO_4 and $CaSO_4$ might partly remain in the ash [100], ending up in different ash fractions.

The main focus in this thesis is on ash formation during char conversion and what remains in the residual ash. SiO_2 is prone to form low temperature melting K-silicates in ash from alkali-rich fuels. The silicates stay in the residual ash, and generally have high slagging tendencies [19, 96, 105, 106]. If CaO or MgO is available, it will to some degree dissolve into the melt. High concentrations of dissolved alkaline-earth metal in the ash melt fuel can lead to increased release of potassium [19, 21, 97]. When the content of calcium and magnesium increase, the silicate generally achieves a higher melting temperature, and the slagging

tendencies can decrease [19, 21, 96, 97, 102]. Contamination in the fuel by certain aluminum-rich clay minerals may also interact with slag formation, producing alkali aluminosilicate with higher melting temperature, which can also reduce slagging tendencies [21].

If there is an excess of basic oxides, primarily potassium or calcium, and depending on the atmosphere and temperature, carbonates will form through reaction with CO_2, in agreement with the stability indicated in Figure 2, and in agreement with chemical phase equilibrium. Carbonates in lignocellulosic biomass ashes are normally calcium carbonates and mixed K-Ca carbonates, while pure potassium carbonates are rarely observed [21]. Their stabilities are, however, limited. Decomposition of carbonates of calcium and potassium in typical boiler conditions occurs between 700-900°C depending on fuel type, and results in the gradual release of K as KOH [97, 100, 107]. Calcium oxide is formed by the carbonate decomposition mentioned, but CaO and/or MgO can also be found in the residual ash due to excess of Ca and Mg compared to reactive acidic compounds.

If the residual ash begins to melt it can produce slag or bed agglomeration in fluidized bed furnaces which can, in part or totally, hinder the conversion process. As mentioned above, the slagging tendencies are highly dependent on the composition of ash-forming elements, the amount of ash and the temperature. The viscosity (i.e., the potential stickiness of the melt) is also important for slagging tendencies [96].

Interactions between ash formation and char conversion

As mentioned above, alkali compounds play a major role in all aspects of ash-related operational problems. On the other hand, some of the alkali components are known to have a catalytic effect on conversion reactions, increasing reactivity of the fuels [108-113]. The mechanism of the "catalyzed" gasification of carbon and coal has been well described in earlier studies [114-117]. Alkaline earth metals (AAEM) and iron are also known to act as catalysts in thermal conversion processes [108, 109, 112]. Most studies agree on the rate enhancing effects of the inorganic elements. In some cases though, the effect might be limited to a certain time point during the conversion process, and results can differ to a certain extent between the studies. Even though some mechanisms have been suggested, observations and hypotheses still diverge.

Other inorganic substances such as silica, alumina and phosphates have been found to lower the reactivity of char [118-122]. Silicates or phosphates have been observed to be formed when potassium (or calcium or another "catalyst") reacts with silicon or phosphorus; potassium is no longer available on active char sites, the catalytic effect is blocked and the reactivity reduced. Simple ratios such as

K/Si [119, 122] or K/(Si+P) [120] have been used to verify and correlate the inhibiting reactions, with ratios exceeding one implying the catalytic potential is still there.

Conversion rate inhibiting effects can also occur from ash layers, hindering access of the oxygen to the char and reducing the apparent reactivity. Studies on coal char found inhibition effects from ash layer for chars with high ash content, and the ash layer diffusion resistance affects the conversion rate and found dependence of the time - temperature profile [123-125]. Reduced char reactivity at high temperature was found for silicon rich straw char, that might depend on molten ash [126]. Branca et al. [127] found that the reduced reactivity was caused by a lower porosity with high amounts of calcium, and a glaze of polymerized products which makes the internal surface of the solid less accessible to the gaseous reagent. Some studies has tried to describe and predict ash inhibition during biomass char conversion [35, 36, 124].

3 Materials and Methods

3.1 Fuels and fuel analysis

In the present thesis, different types of lignocellulosic biomasses have been used, with and without thermal pretreatments. All basic fuel analysis was performed by external certified laboratories.

In the study reported in Paper I, thermally pretreated wood chips from stem wood of Norway Spruce were used. Wood chips, torrefied at pilot scale, were supplied from a pilot scale reactor with a maximum capacity of 20 kg/h. The torrefaction setup and procedure is described elsewhere [61, 128].

In the study reported in Paper II, wheat straw and wood from Scots pine were used and the fuels were dried at 105°C, milled, and sieved into different sized fractions (125-150 μm, 400-425 μm, 600-630 μm).

Industrially produced pelletized fuels were used for the studies reported in Papers III-V; pelletized poplar wood (Papers III and V) and wheat straw (Papers III and IV). The pellets were 6 mm in diameter and the length of the pellets used was adjusted until each pellet tested weighed 600 mg ±5%.

More details of the fuels can be found in the respective paper.

3.2 Experimental setups

In the studies presented in this present thesis, thermal conversion was performed primarily in three types of facilities. A drop-tube furnace (DTF) was used for high heating rate devolatilization of fuel particles (Paper II). The char samples were then used for gasification reactivity studies in a thermogravimetric analyzer (TGA).

In the studies reported in Papers III-V a laboratory scale single pellet furnace equipped with an analytical balance was used, enabling it to be used as a large-sample thermogravimetric analyzer. This setup enabled time-resolved studies of conversion rates and quenching for external analysis of ash formation and transformations at single pellet level.

A domestic pellet boiler was used in the study presented in Paper IV, as a complement to single pellet combustion, to examine the interactions within a batch of pellets on the ash melt formation.

3.2.1 Drop-tube furnace

The drop-tube furnace (DTF) used for char preparation, presented in Paper II, was located at RISE Energy Technology Center (ETC) in Piteå, Sweden. The DTF allowed control of temperature, atmosphere and estimated reaction time. In short, it consisted of a water-cooled injection system for gas and particles (described in detail elsewhere [129]), a vertical reactor tube, and a quenching sampling probe. The alumina (Al_2O_3) reactor tube had an inner diameter of 50 mm and a height of 2.1 m, sealed with endcaps at both ends. A furnace controlled the temperature with five electrical heaters and the atmosphere was controlled using mass flow controllers, which maintained a constant laminar flow of gas downwards through the reaction tube. The water-cooled probe was inserted from the bottom of the reactor, enabling simultaneous sampling of solid material and quenching of reactions; particle residence time could be varied by changing the fall height inside the reactor. Two parallel cyclones were mounted at the end of the probe to collect the char particles. The gas flow was then pumped through a glass fiber filter setup before arriving at the extracting vacuum pump.

Figure 3 presents images taken during the experiments with the DTF at ETC. The DTF and the settings are described in more detail in Paper I and in papers by Holmgren et al. [76] and Wagner et al. [130]. After the chars were prepared in the DTF, they were used for gasification reactivity studies in the TGA.

When studying rapid pyrolysis or gasification, a DTF has some advantages over a TGA with its capacities for high heating rate and short residence time. The TGA is not applicable at high heating rates because of the risk of undesired mass- and heat-transfer limitations [131]. To be able to study the properties of char under these conditions, with behavior similar to that for an entrain flow gasifier, a DTF was used for the char preparation. The DTF allows individual particles to be exposed to a consistent atmosphere and minimizes inter-particle effects. The TGA was used for the detailed gasification characterization of the chars, not enabled by the DTF. However, a drawback with this approach is that the reactivity is known to be affected by the treatment of the char samples, when the samples are first quenched cooled, and then have an annealing step before the gasification [125, 132, 133]. This effect limiting the direct application of the absolute value of reactivity, but still comparison between samples can give valuable information.

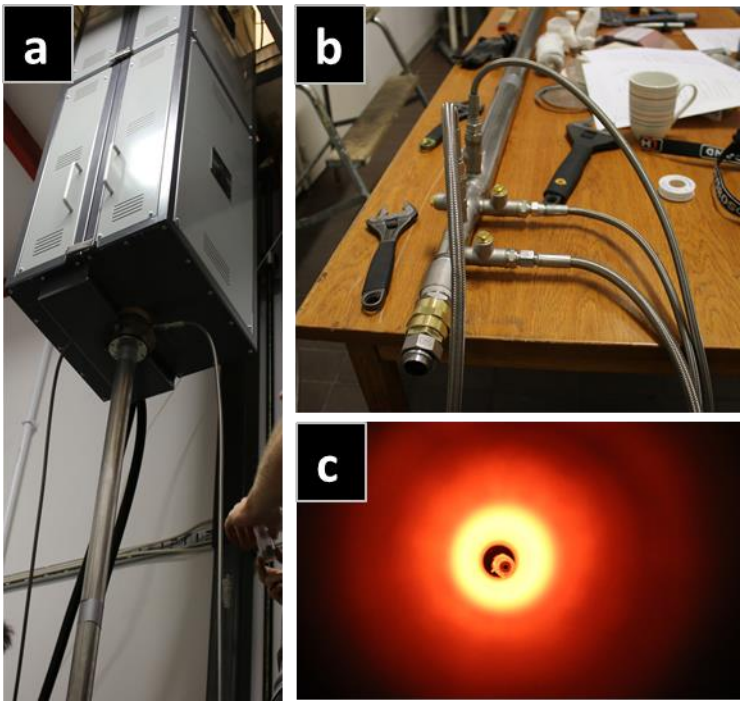

Figure 3. a) DTF with the furnace and the sampling probe underneath, b) sampling probe, showing the water cooling connections (when in operation followed by the cyclones), c) image taken into the hot environment from below, showing the bottom of the cooled fuel injection tube.

3.2.2 Laboratory scale single pellet furnace

An in-house constructed, laboratory scale, single pellet furnace located at TEC-lab, Umeå University was used for single pellet studies. The furnace was equipped with an analytical balance, enabling use as a large-sample TGA. The reactor consisted of a furnace, internal dimensions 200×130×130 mm, with electrical wall heaters, and a quenching tower separated from the furnace zone by a slide hatch. The pellet was placed in a basket folded from a platinum net (platinum to avoid oxidation of the basket and to avoid interactions between the fuel ash and the basket), hanging in a wire from the analytical balance at the top of the reactor. The sample was moved between the hot furnace and the quenching tower by moving the reactor vertically up and down. The quenching tower was purged with N_2. The gas to the furnace was supplied to the bottom of the furnace, preheated and directed upwards by a honeycomb structure used as a flow straightener. An observation window in the front of the furnace made it possible to optically record the conversion process. Figure 4 shows photos of the reactor and the basket. The single pellet reactor was used in the studies reported in Papers III-V and described in more detail therein. The equipment has also been described and used in similar ways by others [57, 134].

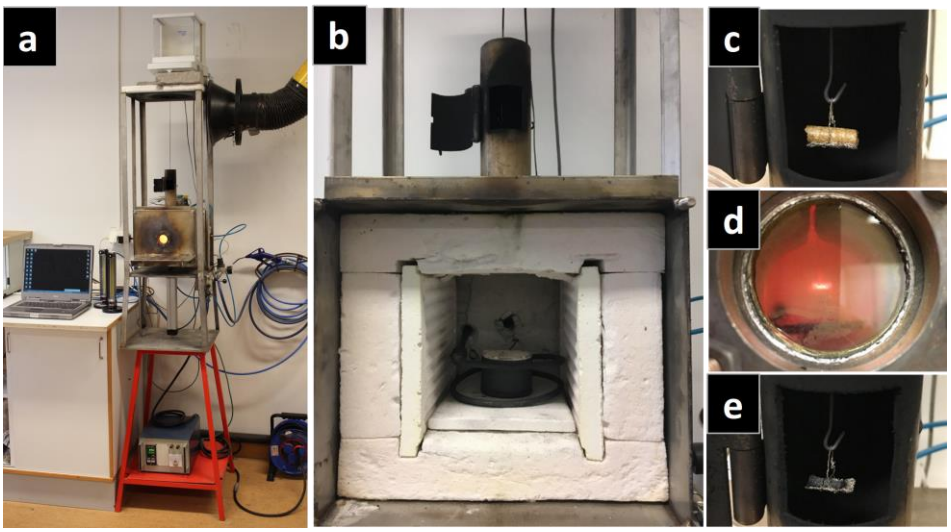

Figure 4. Laboratory scale single pellet furnace equipped with an analytical balance (large-sample TGA). a) picture of the furnace, b) opened showing the oven with insulation and the gas preheating loop, c) wheat straw pellet before d) during and e) after combustion at 700°C.

3.2.3 Domestic pellet boiler

In Paper IV, a domestic pellet burner located at TEC-lab, Umeå University, was used. The burner, manufactured by EcoTec, Sweden, had a nominal effect of 20 kW and was installed in a reference boiler of the same type as the ones used in Sweden for national certification tests of domestic pellet burners, and used in earlier work [96, 135]. The burner was under-fed by a feeding screw that pushed the fuel up to the rim. The ash is pushed by the fuel from the burner down to the boiler floor. Figure 5a presents a photo of the domestic pellet boiler, together with the appearance of the burner during combustion of standard wood pellets (b) and wheat straw pellets (c), visualization of the slag that is formed during combustion of the straw.

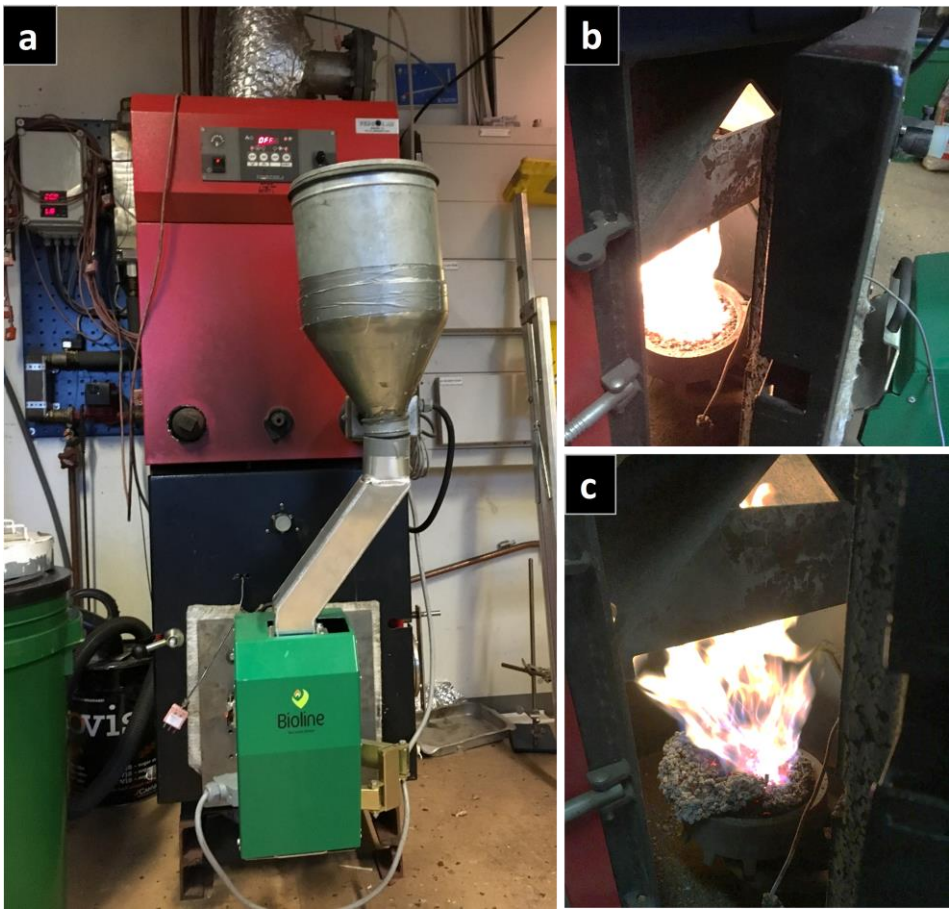

Figure 5. a) Domestic pellet boiler, b) combustion of standard wood pellets, c) combustion of wheat straw pellet showing the slag formed.

3.3 Analytical methods

In the present thesis, the fuel was characterized and analyzed using traditional fuel analysis, thermogravimetry, SEM-EDS, powder X-ray diffraction (XRD) and a more novel method for biomass particle characterization, X-ray micro-tomography. A thermogravimetric analyzer (TGA) was used in the studies presented in Papers I and II to measure weight loss vs. time. This is sensitive to low-level weight changes. The technique has been used for comparing decomposition profiles and for kinetic studies of intrinsic reaction rate during char gasification.

SEM was used to provide high-resolution images; this method was combined with X-ray micro-tomography to enable 3D analysis of char and ash morphologies.

Scanning pellets quenched at different times during the conversion process generated time-resolved data on char conversion and ash formation. X-ray micro-tomography was used in the studies presented in Papers III and IV.

SEM-EDS provides data on both morphology and the elemental composition of samples, and was used in the studies presented in Papers II-V. For the phase compositions, this data was complemented with powder XRD, providing information on which crystalline compounds or phases are present in the sample (Paper V).

3.3.1 Thermogravimetric analyzer

A thermogravimetric analyzer (TGA, Q5000IR, TA Instruments), located at the Thermochemical Energy Conversion laboratory (TEC-lab), Umeå University, was used in the studies presented in Papers I and II. The TGA and autosampler with samples (Paper I) are shown in Figure 6. Samples of milled, thermal pretreated pine wood chips undergoing thermal conversion in an inert atmosphere were used in a study presented in Paper I. In another study, reported in Paper II, chars were gasified in a CO_2 atmosphere. More details and information about the conditions can be found in Papers I and II.

The TGA records the weight change as a function of temperature and time. The technique is very useful for analysis of the composition of complex materials using their thermal stability; this method is even standardized [136]. The curve shape, or the shape of first- or even second-time or temperature derivative of the weight loss, can also be used to evaluate fuel properties at different temperatures and atmospheres (Paper I).

In the study described in Paper II, the reactivity of biomass chars during gasification were analyzed. The intrinsic reaction rate, i.e. the rate of chemical reaction without heat and mass transfer limitations, is important from a theoretical viewpoint [90]. Larger biomass particles affect the apparent reactivity through diffusional effects [92]; this also applies to a large sample mass or a deep sample with a significant internal diffusion resistance [90]. To carry out the experiments in kinetic regime, confounding effects including heat transfer problems must be reduced by using a low heating rate and small sample mass [7, 91, 93]. Therefore, biomass chars were ground into very fine powders for intrinsic kinetics estimations. The char was distributed on the crucible as a thin layer to avoid the transport processes influencing the DTG curves.

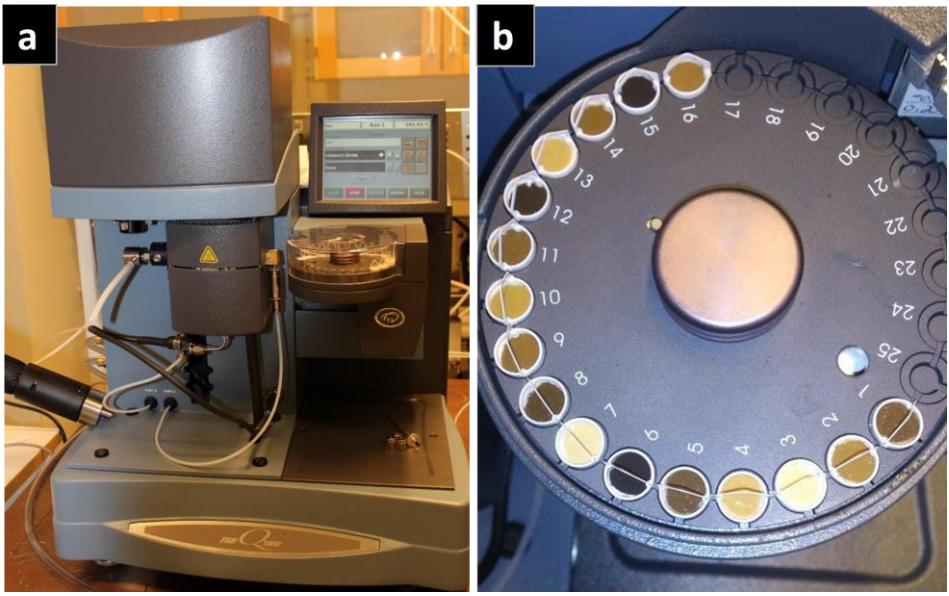

Figure 6. a) TGA with autosampler, b) the sample holder with samples from different degrees of thermal treatment (Paper I).

3.3.2 Scanning Electron Microscopy

In the study presented in Paper II, the scanning electron microscopy (SEM) used was a Philips XL-30 environmental scanning electron microscope equipped with an EDAX energy dispersive detector (EDS), all located at TEC-lab, Umeå University. In Papers III-V, sample morphology was analyzed by variable-pressure scanning electron microscopy (VP-SEM; Carl Zeiss Evo) at the Department of Applied Physics and Electronics, located at the Umeå Core Facility for Electron Microscopy (UCEM) at the Chemical Biological Centre (KBC), Umeå University. Elemental analysis was performed using an energy dispersive X-ray spectrometer (EDS; Oxford Instruments X-Max 80 mm^2). The SEM was usually operated at 15 kV with probe current of 200-300 pA. Backscattered Electron (BSE) images were obtained, visualizing the compositional contrast through the distribution of different elements with different atomic numbers, thereby generating an image of the composition and morphology of the sample.

Using EDS the different elements and their relative proportions can be identified. This is based on Henry G. J. Moseley's findings (1913, 1914), that wavelengths of characteristic X-rays have a systematic mathematical relationships (variations) correlated to emitting atomic numbers [137, 138]. The sample (solid) is bombarded with a focus beam of electrons and the incident electron knocks the inner shell electron out of its orbit. An electron from an

outer atomic shell takes its place so that the atom returns to its normal state giving off a specific amount of energy in the form of X-rays. For example, removal of the K shell electron, with the L shell electron taking its place produces Kα X-ray. In this way, an X-ray spectrum is emitted by the sample, and EDS analyzes the X-ray spectrum based on this energy. This provides a local chemical analysis.

Molten ash particles and chars were mounted in epoxy resin and dry polished with silicon carbide paper for cross-section analysis, whereas powdery fractions were dispersed on carbon tape. Average elemental concentrations of main ash-forming elements were determined based on five or more spot or area analyses for each fraction. Chlorine is present in the epoxy and was therefore excluded from the EDS analysis in those cases in which epoxy was used.

3.3.3 X-ray micro-tomography and image analysis

X-ray micro-tomography was used with two different applications in the studies presented in Papers III and IV: Synchrotron-based hard X-ray micro-tomography and micro-computerized tomography (micro-CT). All micro-tomographic setups consist of an X-ray source, a rotating sample pod, a scintillator (which converts X-rays to visible light) and an optical detector. When the sample rotates, images of 2D projections from the part of the sample that faces the detector screen at that moment are taken at fixed intervals. Using numerical reconstruction, these projections are transformed into a 3D image [139]. The density and atomic number Z of the elements in the scanned object affect the absorption (or attenuation) of the X-rays passing through the sample, and the resulting images constitute gray scale values that correspond to a quantitative measurement of the linear X-ray absorption coefficient (μ).

Synchrotron-based hard X-ray microtomography

Synchrotron-based hard X-ray micro-tomography was performed using Beamline 8.3.2 at Advanced Light Source (ALS), Lawrence Berkeley National Laboratory (LBNL), Berkeley, California, USA. Synchrotron radiation is electromagnetic radiation emitted by high-speed charged particles, electrons. At the synchrotron ring facilities these electrons are accelerated in a magnetic field to near the speed of light, producing synchrotron radiation with a very intense spectrum of continuous X-ray wavelengths. The X-ray source at ALS provides synchrotron radiation from a 1.9 GeV electron beam within a 6 Tesla superconducting bend magnet; at the source point of Beamline 8.3.2 the field strength is 4.37 Tesla yielding a critical energy of 11.5 keV [140]. Significant flux out to >50 keV is available for penetration through samples. With the high X-ray flux of a synchrotron, imaging of dense samples at micrometer-scale resolution is possible. Figure 7 shows a schematic sketch of the sample scanning procedure

and setup inside the hutch at ALS Beamline 8.3.2 [141]. The X-ray source beam (1) for this study, with an X-ray energy of 20 keV, was projected through the sample (2); the sample was mounted on a kinematic mount that was attached to a rotation stage (3). X-rays passing through the sample are converted to visible light using a high-resolution crystal scintillator (4) that converts X-rays to visible light which is redirected by a mirror (5) through lenses (6). The visible light is then projected onto the CCD camera (7) for image collection. The raw 2D projection image recorded by the camera corresponds to a parallel projection of the sample onto the scintillator by the X-ray beam. In tomographic scans, a series of projection images are taken while the sample is rotated through at least 180 degrees (during a full scan at an angular step of 0.175° resulting in 1,025 2D images). These images are transformed using a mathematical procedure for tomographic reconstruction and a software algorithm developed at LBNL. This results in a stack of transverse images (bottom right) that are used for the 3D reconstructions and analysis. The responses from scanning and reconstruction are grayscale values of the voxels, which correspond to a quantitative measure of the linear absorption coefficient (μ), and provides images in which bright spots have high optical densities and black spots have low optical densities.

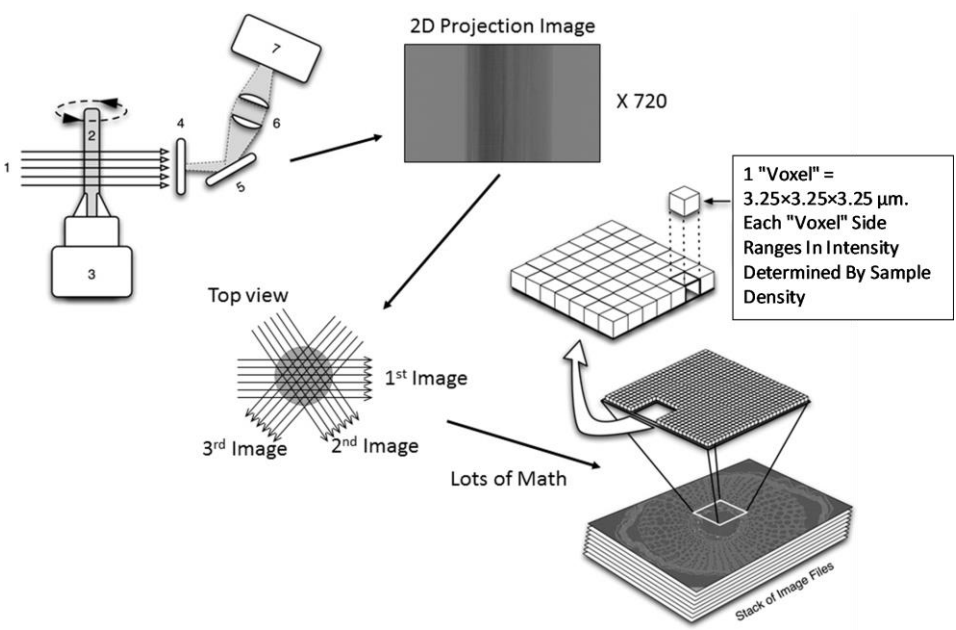

Figure 7. Schematic sketch of sample scanning procedure and setup inside the hutch at ALS Beamline 8.3.2. Reprinted with permission from McElrone et al. [141]. Copyright (2013) Journal of Visualized Experiments.

Micro-computerized tomography
In contrast to synchrotron large-scale facilities, commercial micro-CT scans can fit into a room, mainly due to their compact X-ray source. The source of the X-ray radiation is the tip of a vacuum X-ray tube, consisting of an anode and a cathode of high atomic weight material (in this case tungsten). By applying high voltage between the anode and the cathode, accelerated electrons (cathode rays) produce X-rays as they strike the anode. More on this technique can be found for example in Wildenschild et al. [142].

The study presented in Paper IV used a micro-CT, GE v|tome|x 240 with a tungsten target and a GE 16" flat panel detector with 2024 × 2024 detector crystals. It is situated at the X-ray facility of the Department of Soil and Environment at the Swedish University of Agricultural Sciences, Uppsala, Sweden, and was used for X-ray images of charred pellets. The images were collected at regular angular intervals during a 360-degree rotation of the samples. Each corresponded to the average of 6, obtained with an exposure time of 133 ms at a tube voltage of 90 kV and an electron flux of 60 μA. The charred pellets were placed inside a sample holder with a 1 mm thick aluminum wall which acted as an optical filter to reduce beam hardening artifacts. The images had a resolution of 6.2 μm in all directions. They were reconstructed from 2,000 radiographs using the GE software datos|x.

Image analysis
Image analysis and visualization of 3D tomographic volumes were performed using the software packages Fiji (Fiji Is Just ImageJ) and Avizo 9.3 (Fei VSG Inc., Burlingham, MA, USA). The analyzes included watershed segmentation, surface rendering reconstructions, and area and volume analysis of the reconstructed micro-tomography images. For each sample, the area of interest was identified, and the background was masked by subtraction. Based on the absorption histogram, segmentation was carried out with threshold <2.0 μ for cracks/cavities, threshold 2.0–4.0 μ for char matrix and threshold 4.0–4.6 μ for ash compounds.

3.3.4 Powder X-ray diffraction
Powder X-ray diffraction (XRD) analysis (Paper V) was performed on a Bruker AXS d8Advance diffractometer in θ-θ mode, Cu Kα-radiation (1.5418 Å) with a line profile and a Våntec-1 detector, located at the TEC-lab at Umeå University. The range for data collection was 2θ 10°-70°. Scan speed was 3° per minute and the rotation speed 10-30 rpm, depending on the sample holder used. With continuous scan and addition of the repeated scans, the total data collection time for each sample was at least 4 hours.

X-ray powder diffraction (XRD) is a technique used to gain information about crystalline phases in solids. A monochromatic beam of X-rays is produced and directed onto the powder samples. When the incident rays interact with the sample, constructive interferences are produced from the diffracted X-rays. The diffraction angle and lattice spacing are related to the wavelength of electromagnetic radiation by Bragg's Law ($n\lambda=2d \sin \theta$) [143, 144]. The sample has crystals that (ideally) are randomly orientated and, by scanning through a range of 2θangles, all possible diffraction directions of the lattice are captured. The sample and the detector are rotated so that more angles are represented, becoming thereby closer to the ideal case, and the intensity of the reflected X-rays is recorded. Each crystalline solid has a (more or less) unique X-ray powder pattern which gives a "fingerprint" of the crystals present in the sample. This can be identified by comparing the pattern with those from known structures. Both the position and the relative intensity of the lines in the pattern are used for identification.

The samples were ground to fine powders, and spread out evenly on the sample holder to ensure random orientation of the crystals. The crystals generate detectable signals at all angles, and this minimizes the background noise. The samples were mounted in plastic holders; samples with small amounts of powder were applied on a silicon crystal low background sample holder. The sample holders were mounted in a rotating sample stage. For the silicon crystal sample holder, a background pattern was collected for an empty holder and was subtracted from the spectra of the samples.

Phases in the sample were identified by comparing the diffraction patterns recorded with those from known structures using crystallographic databases. The initial qualitative identifications were made by the PDF-2 databank [145] together with Bruker software. Semiquantitative information on the present crystalline phases were acquired from analysis using the Rietveld technique and crystal structure data from ICSD [146].

Non-crystalline (amorphous) phases cannot be directly identified with XRD. However, amorphous phases are common in, for example, silicon-rich samples and can in some cases be identified as broad peaks. XRD analysis was used for the study presented in Paper V, where samples from poplar wood ash were analyzed without indication of large contributions from amorphous phases.

3.4 Data analysis

3.4.1 Multivariate data analysis

The primary purpose of multivariate data analysis (also called chemometrics in the context of spectral data from typical chemistry applications) is to generate an overview and to see relationships between observations and variables of large datasets as well as to predict new data. When the number of samples is much lower than the number of variables, classical statistical methods (or univariate analysis) becomes delimitated or improper [147]. If univariate analysis is used on multivariate data (large datasets), there is a risk of false results or loss of information, because the information can lie in the correlation between the variables and not in the individual signal. With the complex composition of lignocellulosic biomasses, the decomposition pattern sometimes has interfering and overlapping variables. In addition, the later part of the conversion is highly dependent on the earlier parts; multivariate data analysis was therefore tested as an alternative to classical curve deconvolution (Paper I). Previous studies have indicated the method to be useful, for example when evaluating the chemical and physical properties of biomass and peat, analyzed by TGA [148, 149], and by Differential Scanning Calorimetry (DSC) and Near Infrared spectroscopy (NIR) [150]. NIR and/or Fourier-transform infrared (FTIR) spectroscopic data with multivariate analysis have recently been proven to work well for accurate characterization of torrefied and charred biomass [151, 152], as well as for predicting the treatment level of furfurylated Scots pine [153]. In the present study (Paper I), multivariate analysis was performed using the SIMCA-P software (MKS Umetrics AB, Sweden, version 13.0). The approach in this study includes Projection to Latent Structures (PLS).

Partial least squares projection to latent structures analysis (PLS) is a commonly used method for regression analysis. PLS finds relationships between blocks of multivariate data, X and Y, maximizes the value of the covariance between the two data sets, computing the first PLS component [154-157]. The remaining covariation between the matrices is the residual, which is used to calculate the next PLS component, with the components orthogonal to each other. New model components can be added to fit the data; however, with too many components, the model might be over-fitted with reduced predictive capacity and a risk of introducing noise. Goodness of fit (R^2) is used to show how well the model fits the data, namely, how much of the variation that is explained. The problem with the goodness of fit is that with more parameters in the model, R^2 can be made arbitrarily close to the maximal value of 1 while the model fails in predicting new samples. Cross-validation (CV) is used for internal validation purposes and a quality measure of the model is estimated with goodness of prediction, Q^2 [158]. The maximum value for Q^2 is 1, which means perfect prediction, while a value

around 0 indicates no predictive ability, with the risk that the model can include noise and a random guess might be the outcome.

Advantageously, an external validation can be performed, by predicting in samples using an external set of samples. When model errors are unbiased and follow a normal distribution the model's ability to predict new samples is assessed by root-mean-square error of prediction (RMSEP) [159], computed as

$$\sqrt{\frac{\sum(Y_{obs}-Y_{pred})^2}{N}}, \quad (1)$$

where Y_{obs}-Y_{pred} refers to the predicted residuals for the observations in the prediction set. RMSEP is calculated for the complete model.

In the study presented in Paper I, PLS was used directly on the time derivative DTG curves for prediction of mass yield, higher heating value (HHV), elemental composition (C, H and O), and content of volatiles of torrefied wood. To explain as much of the variation as possible in the first component, the coordinate system was mean-centered, i.e. moved and centered to the origin by subtracting the average from each variable, or column of the data matrix [147, 160].

3.4.2 Thermodynamic equilibrium calculations

In the present study, FactSage™ 7.1 software [161, 162] and databases FactPS, FT Oxide and FT Salt were used for equilibrium calculations. The method with thermodynamic equilibrium calculations is based on well-established thermodynamic principles, including minimization of the Gibbs energy of the system, calculated using the software and databases (if data exist for all the phases considered) [163]. This can provide extensive information on the system that is studied and the predicted ash reactions, and can be used to understand the chemical behavior of complex systems. However, limitations with the method need to be considered when interpreting the results from the analysis. The system is assumed to be in equilibrium and that implies infinite reaction times and perfect mixing. There is no consideration of chemical kinetics and reaction rates. There is also a risk of a potential lack of data. The results are also sometimes dependent on the choice of solution model and databases.

In the study presented in Paper II, calculations and thermodynamic data were used to support a discussion on chemical phase equilibrium in the ash. The method was also used for discussion and assessment of the results in Paper IV. In Paper V, calculations and thermodynamic data were used when planning the experiments to predict the ash reactions under different conditions, and later also for evaluation and discussion of the results.

3.4.3 Viscosity estimation

The viscosity toolbox in FactSage™ 7.1, together with the MELTS database, was applied to the wheat straw ashes in Paper IV for viscosity estimation [164-166]. Calculations were made based on the relative composition of SiO_2, CaO, MgO and K2O, given by the SEM-EDS analyses, in the ashes around the char or the residual ash for the various samples. Assumption was made that all ashes were melted. For these calculations, it was assumed that temperatures were according to temperature measurements by Fagerström et al. [134]; for a furnace temperature of 700°C, the pellet temperature was approximated to 900°C and the furnace temperature of 1,000°C to 1,100°C.

4 Results and discussion

4.1 Fuel devolatilization and char morphology

Results from devolatilization of fuel particles were reported in several of the papers (I-IV). Different fuels and devolatilization conditions affect the decomposition and morphological changes of the particles. Fuel particles and chars from different experiments are presented in Figure 8, both from small particles of pine and wheat straw exposed to devolatilization at high heating rate, and pelletized poplar exposed to devolatilization in an isothermal single pellet furnace, in this case operated at 1,000°C.

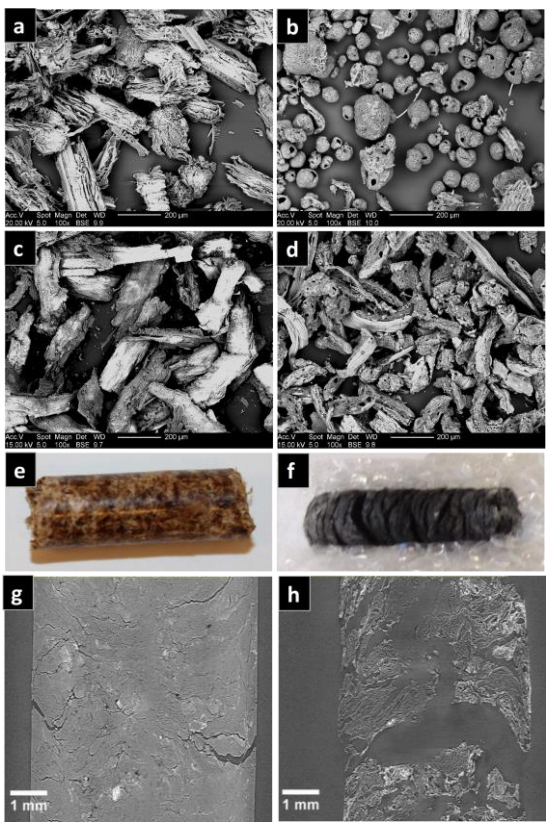

Figure 8. Fuel particles (left) and chars (right) using different types of fuels and devolatilization conditions. SEM micrographs of a) pine particles (size 125-150 µm), b) chars from the pine particles devolatilized at high heating rate in a DTF at 900°C. SEM micrographs, of c) wheat straw particles (size 125-150 µm), and d) chars from the wheat straw devolatilized at high heating rate in a DTF at 900°C. Photos of e) poplar pellets, f) char from poplar pellet after devolatilization in a single pellet furnace at 1,000°C. Images from synchrotron-based hard X-ray micro-tomography showing cross-sections of g) poplar pellet, and h) the char after devolatilization of a poplar pellet in a single pellet furnace at 1,000°C.

The main components of biomass (hemicellulose, cellulose and lignin) play individual roles in biomass decomposition behavior. In an inert atmosphere and at low or moderate heating rates, this behavior is reflected in the weight loss curve, and can be associated with the component dynamics. In the study presented in Paper I, with the aim to predict fuel properties based on thermal decomposition behavior, a PLS model was developed based on the shape of DTG curves (the time or temperature derivative of the mass loss, TGA). The weight change of a sample heated at controlled rate depends on the composition of the sample, and by using the DTG curve shape for evaluation, some fuel properties, e.g. mass yield, heating value, volatile content, and elemental composition could be accurately predicted by the PLS model. Wood chips, thermally pretreated under different conditions in a torrefaction pilot plant [61, 128] were milled and analyzed in the TGA. The thermal pretreatment caused shape changes in the DTG curve, corresponding to change in the relative abundance of the main components of wood, i.e. hemicellulose, cellulose and lignin [61, 63, 167], but in the algorithm they were treated as multivariate spectral data without any compositional information. Figure 9 presents DTG curves for some of the samples used, where higher sample numbers indicate lower severities of thermal pretreatment.

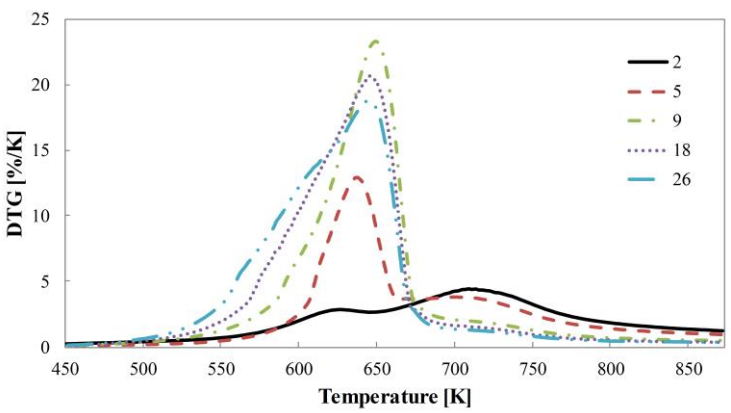

Figure 9. DTG curves for thermally pretreated wood, with an increase in sample number corresponding to decreased severity of thermal pre-treatment. Reprinted with permission from Strandberg et al. [168] (Paper I).

A well-fitted PLS model was obtained with tree-significant components, with the variation of all variables well explained ($R^2Y = 0.992$, $R^2X = 0.991$); all variables could also be predicted with good accuracy ($Q^2 = 0.988$). This indicated that the model fitting was of good quality and new data could be well predicted. Q^2 was estimated by cross-validation. The best information lay within an area representing mostly hemicellulose decomposition, but statistically significant

data was also found for the two other pseudo-components. The multivariate approach had an error of prediction of 2.7%.

A conventional curve deconvolution approach, numerical least square curve fit (NLS), which is also based on the change in shape of the DTG curve, corresponding to changes of the relative occurrences of the main components of wood (i.e. hemicellulose, cellulose and lignin), was used for comparison with the PLS model. If the samples were not severely pre-treated (remaining constituents were mostly intact), the NLS approach worked satisfactorily. However, with all samples included, the model gave a weaker performance compared to the multivariate approach and resulted in a 29.4% error. The performance of the multivariate approach was more flexible compared to the reference NLS method, but a potential disadvantage for the PLS model is the need for an accurate calibration set and potential sensitivities to sideways data shifts possibly caused by e.g. variations in contents of inorganic elements known to affect thermal stability. If this is not accurately accounted for in the calibration, the multivariate model could be influenced negatively. In contrast, the NLS method is relatively insensitive to sideways movement of data. For PLS models, it is important to use calibration data of good quality, and a majority of the error in this model is presumably caused by uncertainties in the actual measurements of the mass yield in the pilot scale torrefaction plant, which was determined to be 4% with a confidence level of 95% [61].

In Paper II, results from char samples prepared by devolatilization of the fuel particles at high heating rate in a DTF at 900°C and 1,100°C are shown. The fuels were pine stemwood and wheat straw with different original particle sizes (small particles of 125–150, 400–425 and 600–630 μm). The char properties were expected to be affected by the heating rate. The estimated volume averaged heating rates for wood particles show that the smallest size range had a much higher heating rate than the other sizes, given the assumptions in the used calculations. During devolatilization, the morphology of the pine wood particles changed with shrinkage and plastization of cell structures, including formation of spheres (Figure 8a-b). The plastization is likely to alter char properties, but SEM analysis showed a similar degree of transformation for all size fractions. Wheat straw particles (Figure 8c-d) exhibited only minor shape changes, and weight loss took place mainly through loss of density. The studies included in the present thesis focus on char and ash properties, but a separate publication from the same experiments, not included in the present thesis, provides more detailed information on fuel particle size and shape transformation during devolatilization [76].

Papers III-IV present results from combustion of pellets from poplar wood and wheat straw in a large-sample TGA at furnace temperatures of 700 and 1,000°C.

A major part of the mass loss occurs during devolatilization, similarly for both fuels. Using microtomographic scanning and reconstruction, detailed grayscale images were obtained, and cracks, internal cavities and denser ash clusters were visualized, revealing that numerous cracks and internal cavities were formed already during devolatilization. This is presented for poplar pellets in Figure 8, showing the poplar pellets before combustion (g) and the char quenched at the end of the devolatilization phase (h). Additional quenching points during devolatilization revealed that the formation of cracks and cavities starts to occur to a great extent already during the later part of the devolatilization phase.

The calculated volume fraction of cavities for poplar and wheat straw pellets during the char conversion phase (at 1,000°C) are shown in Figure 10. Based on data on average diameters of the chars, shrinking appears to be similar for both poplar wood and wheat straw at both temperatures during devolatilization (Figure 10). For the first part of the char oxidation (between quenching points 1–2) the outer diameter remained constant for all samples. For poplar pellets, the diameter began to decrease again after quenching point 3, at around 40 wt% of the char combustion. For wheat straw (WS) the shrinkage behavior varied depending on combustion temperature; WS700 kept its outer diameter quite constant while WS1000 shrank continuously after quenching point 2, probably due to the ash forming a rigid net structure at the lower temperature, but melting at the higher temperature.

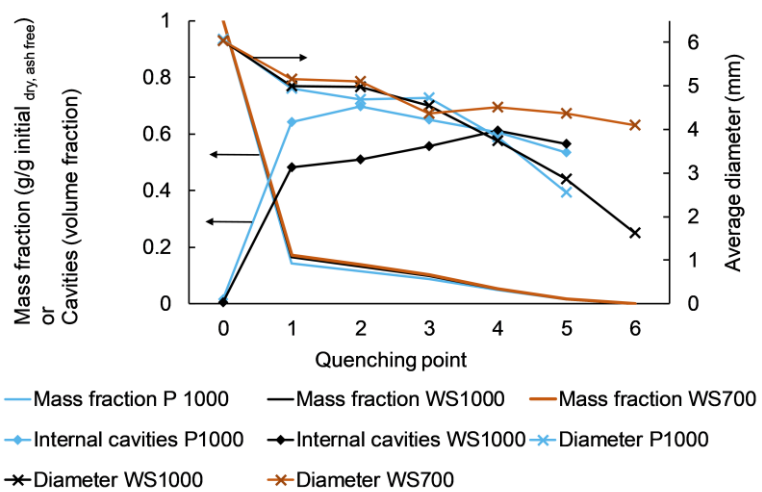

Figure 10. Mass fraction, volume fraction of internal cavities, and average diameter for poplar pellet (P), wheat straw pellet (WS), and the corresponding char samples from different quenching points at furnace temperatures 700°C and 1,000°C (Papers III-IV). Note that quenching point 6 in this figure is at full conversion, corresponding to quenching point 7 in Paper IV.

Watanabe et al. [169] found that the pore structure of raw wood cylinders from hardwood and softwood was preserved after heating, and gasification of the chars did not show any formation of large cavities and cracks. However, in another study by Pattanotai et al. [170], many pores were shown to exist in the wood char, and relatively large pores (2–3 μm) were visualized using X-ray CT technique, with the 3D image confirming that the pores mainly align along the axial direction (grain direction). This anisotropic structure influences the transport of gasifying agents into the inner char during gasification. The appearance of pores increased with a higher heating rate; the diameter decreased less or increased due to swelling; and the density was lower. Results in Paper III indicate a more complex situation for the conversion of pelletized biomass compared to that previously described for conversion of uncompressed biomass particles, both in regard to the extensive formation of large cavities and cracks during conversion, not only along the axial direction, and from the viewpoint of ash formation. Fixed-bed combustion with larger particles is often modelled in a shrinking core mode, with an unreacted particle/core [23-25, 30, 32-34]. Only a few studies have been found focusing on pellet conversion and none of them take into consideration the large grain separation and formation of cracks and cavities reported in the present thesis. Instead these studies are based on assumptions of the shrinking core model with different reacting layers [32-34]. Accurate description of pore development and change in density during conversion may be needed also for densified biomass; different simplification strategies for wood logs and pellet for devolatilization models have earlier been suggested by Biswas et al. [34]. With the large cavities and cracks that occurred during the conversion, the conversion rates will probably be affected by increased active char surface area and increased gas transport to and from the inner part of the pellets. This will probably also affect the temperature gradient.

In some oxidation models, the particle is covered by an ash layer and take into account some properties such as ash porosity and tortuosity [30, 35-37]; in other models the ash layer remains attached and inert [23, 26], but in most cases the ash is disregarded [24, 27] or not even mentioned. For improved models, incorporation of ash properties will become necessary and possible, but for fuels with high ash content and relative low-melting point of the ash, modelling will be extremely complicated [171]. For large-scale simulations of gasifiers and boilers, the models need to be simplified to a certain degree, and predictive models can be formulated without these considerations. However, these simplifications also mean that the effects of different ash properties or different defragmentation behaviors of fuel particles cannot be accurately predicted.

4.1.1 Char conversion rate

The char conversion rate are important for the design and development purpose for gasifiers and combustors, and as describe in 2.2.3, the char conversion is the limited step of the conversion process. Here, some results from papers II, III and IV of char conversion rates from different types of conditions and fuels are presented.

In paper II, results can be found from char samples from pine stemwood and wheat straw prepared by devolatilization in the DTF were analyzed for reactivity by TGA under isothermal gasification conditions. No pronounced effect of DTF temperatures on char reactivity was found within the range tested. Reactivity dependence on original particle size was found only for small wood particles (original particle size of 125-150 μm) that had higher intrinsic char gasification rates, which might be explained by a higher heating rate in the DTF for the smallest pine wood particles compared to the larger ones. For the wheat straw particles, the reason to the non-existent difference between the particle sizes might depend of that the interior temperature histories might be very similar among the used size ranges, the particles were flake-like and the smallest dimension was far smaller than the sieve size.

Wheat straw and pine stemwood show significantly different conversion and reactivity profiles. Figure 11 presents the char conversion profiles of pinewood (a) and wheat straw (b) char powders vs. normalized time for different gasification temperatures (700 - 900°C). Pine wood char show an increased reaction rate in later part of char conversion, with a clear dependence on gasification temperature. With increased temperature the effect seems to diminish, and totally disappears somewhere between 850 and 900 °C. These trends might be explained by chemical phase transformations of catalytically active potassium carbonate taking place in that temperature range, others have described this mechanism [116, 172]. As mention above, wheat straw char show a decrease in char conversion rates at later stages of the conversion, and more deactivation was observed with increased temperature, this coincide with more extensive melting of residual ash. Similar observations for silicon and phosphorus rich fuels has been described as deactivation of primarily catalytic potassium in the ash [119-122] and discussed further in section 4.2.

The study in paper II was aimed to measure the conversion rates in the kinetically controlled regime (Regime I), and therefore the mass transports with diffusion through the ash layer buildup on full size char particles is an aspect not covered, and that is addressed in paper III-V.

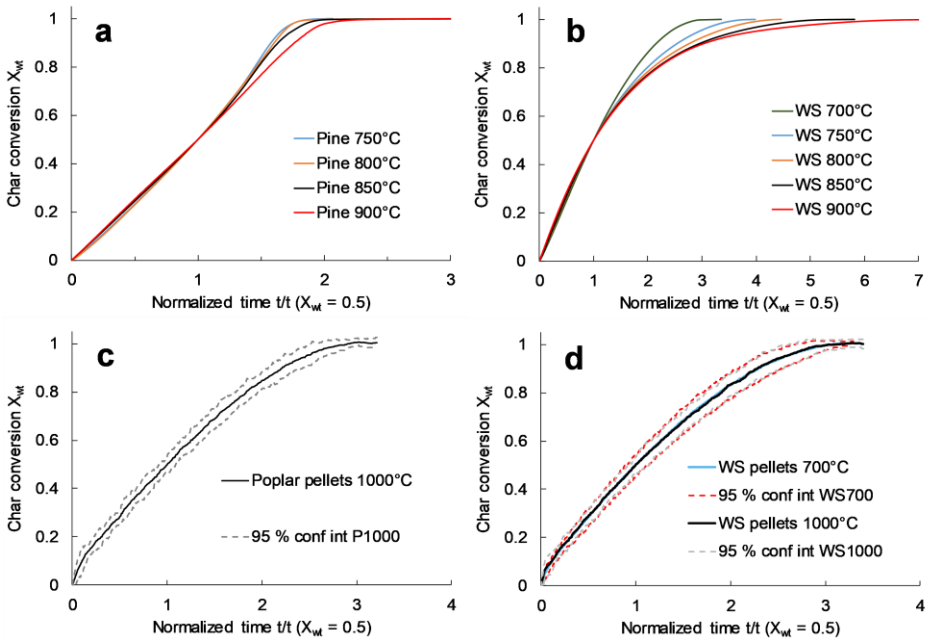

Figure 11. Char conversion vs. normalized time for gasification at different temperatures of char powders (with initial particle size of 125-150 µm, and devolatilized in DTF at 1,100°C) from a) pine wood, and b) wheat straw, and combustion of chars from c) poplar pellets at 1,000°C and d) wheat straw pellets at 700°C and 1,000°C. Data from papers II-IV.

Papers III-V report on results of pellets from poplar wood and wheat straw combusted in a large-sample TGA. The differences in conversion profiles between the fuels were small but significant, with a 12% longer total conversion time for wheat straw pellets during combustion in dry air at 1,000°C. Char conversion is plotted against a calculated normalized time (time/time for X_{wt} = 0.5) in Figure 11. The conversion rates for pellets are highly affected by transport processes, and can be placed in regime III, with the mass loss rate controlled mainly by boundary-layer diffusion. Figure 11 d) shows that the char conversion profiles were similar for the different temperatures for wheat straw. The formation of the melt is different for the different temperatures, but the possible prohibiting effect from the melt on the contact between the char and the oxidation agent appears to be similar for the different temperatures. The surface of the wheat straw pellets at high temperatures was only partially covered by the melted ash (detailed in section 4.2.1), which might explain why wheat straw pellets only showed a slightly longer total conversion time compared to poplar wood; the char conversion profiles also appeared similar. However, some limiting effect from the ash layer was found.

4.2 Ash formation

In the present thesis, different lignocellulosic biomasses were used for studies on ash formation and its influence on fuel conversion. Wheat straw represented an agricultural residue, with ash-forming elements dominated by silicon and potassium; pine and poplar represented woody fuels, with calcium and potassium as the dominating ash-forming elements.

4.2.1 Si-rich silicate forming fuels

Severe slagging problems in bottom ashes are expected from e.g. the wheat straw used in the present thesis, which contains high amounts of silicon, potassium and calcium prone to form low temperature melting silicates during combustion or gasification. Slag formed is mainly restricted to the oxide-silicate system [21]. In Paper II, an extensive melting of the residual ash was seen with gasification of powder from wheat straw char, and the formation of melt increased with temperature. For the lower temperatures (700-750°C) the ash residue was loosely sintered, while at temperatures over 850°C the ash residue was completely melted. The decrease in normalized conversion rate with increasing gasification temperature seen in a later part of the conversion in Figure 11 was probably caused by the melt formation, which limited access of the oxidizing agent to the remaining char.

Interrupted gasification experiments were performed at a temperature of 850°C, and Figure 12 shows the morphology of wheat straw char at partial conversion, with signs of partial melting of the ash-forming matter already at X_{wt}=0.25 (a). At the end of the gasification process (b) almost the entire sample appeared to be melted and, probably, char remained almost totally encapsulated by the dense layer of molten gasification residue.

SEM-EDS analyses performed on char and ash residues demonstrated that silicon followed by potassium and alkaline earth metals dominated the composition. A significant part of potassium was released during pyrolysis in DTF, and during char conversion and ash formation potassium continued to be released. Calcium and magnesium can increase the melting temperature for ashes rich in potassium and silicon, but in this case the amounts of calcium and magnesium were low, and the melting temperature remained low.

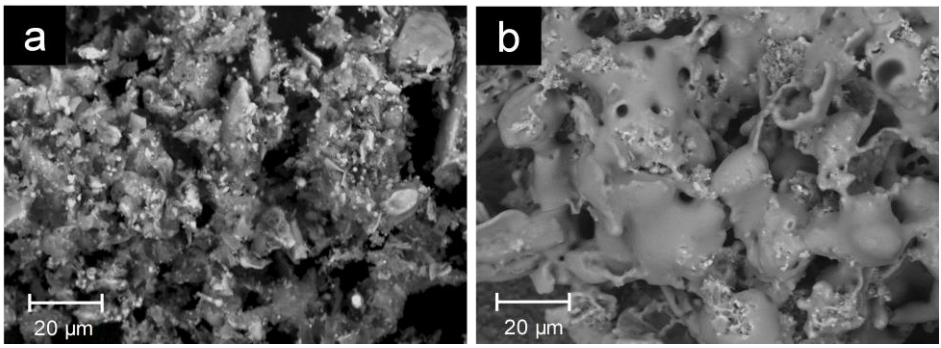

Figure 12. Backscattered electron pictures of char/ash residues from interrupted TGA gasification experiments of wheat straw char powder at 850°C at conversion of a) X_{wt} = 0.25, and b) X_{wt}=0.90. Adapted with permission from Effects of Pyrolysis Conditions and Ash Formation on Gasification Rates of Biomass Char, Strandberg et al. [173] (paper II). Copyright (2017) American Chemical Society.

An important observation in wheat straw char gasification, primarily in the later part of the conversion, was a layer of molten ash that could have a pronounced physical inhibiting effect, even with very thin layers of char powders of small particle size. Efforts to evaluate intrinsic kinetic parameters using TGA can be obstructed by the molten ash layer, inducing a strong diffusion barrier that might affect the reaction rate. Other fuels with high ash content and ash composition with low melting temperature could have the same problems with diffusion limitations, moving the reaction outside regime I conditions. When pellets from wheat straw were combusted in a single pellet furnace (Papers III and Paper IV), complete char encapsulation by ash layers limiting char burnout was not found. The same pellets were also combusted in a domestic pellet boiler (Paper IV), and neither here was complete encapsulation found to any great extent. The pellets were combusted at two furnace temperatures, 700°C (WS700) and 1,000°C (WS1000). However, in an earlier study using the same furnace it was found that the pellet temperature was about 200°C and 100°C higher than the isothermal set points of 700°C and 1,000°C during combustion. There is a distinct difference in the structure of the silicate melt formed during the char conversion, which is clearly shown both in SEM micrographs (Figure 13) and visualized using 3D reconstructions from micro-tomography scans (Figure 14). The 700°C samples (Figure 13 a-c and Figure 14 a-b) formed a rigid ash structure, with the ash formed as net of streaks or small beads surrounding the char. The shape and size of this ash structure remained almost the same as that of the char when the ash started to form on the surface and persisted during conversion. The char part became smaller and smaller, finally disappearing in the center of the structure at full conversion.

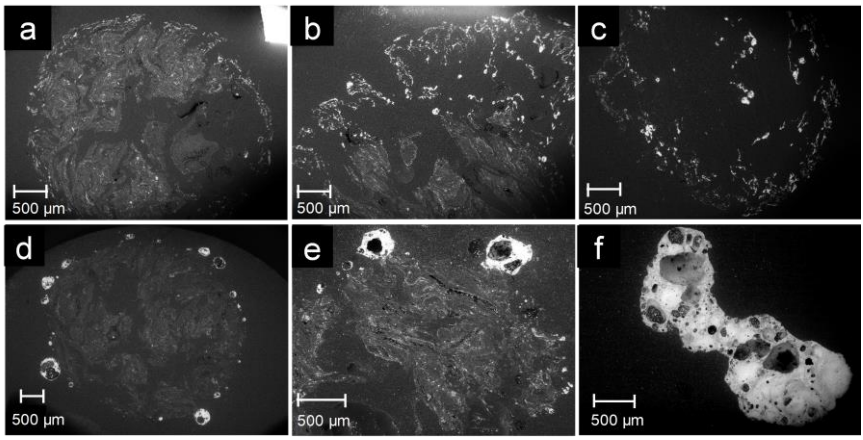

Figure 13. SEM micrographs of char and ash from combustion of wheat straw pellets at 700°C: a) WS700 X_{wt}=0.71, b) WS700 X_{wt}=0.93, c) WS700 X_{wt}=1 (full conversion), and at 1000°C d) WS1000 X_{wt}=0.68, e) WS1000 X_{wt}=0.91, and f) WS1000 X_{wt}=1 (full conversion).

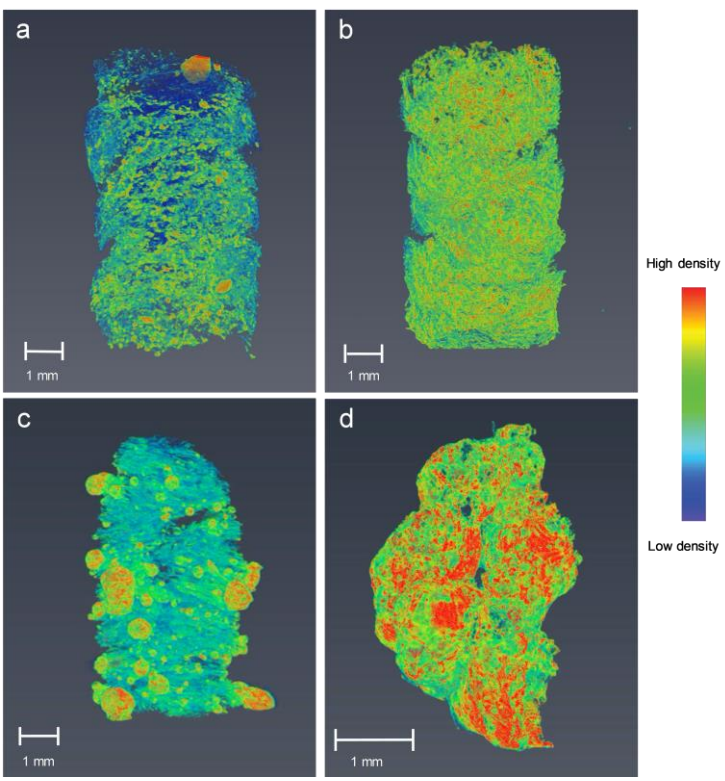

Figure 14. 3D reconstructions with color mapped by X-ray absorption (density) from 2.0 µ to 4.6 µ, a) WS700 at X_{wt} = 0.93, b) WS700 at X_{wt} = 1 (full conversion), *c) WS1000 at X_{wt} = 0.91, and d) WS1000-7 at X_{wt} = 1 (full conversion).*

For the 1,000°C samples, the melt was concentrated in bubbles, and these bubbles increased in number and size as the conversion proceeded, as can be seen in Figure 13 d-f and Figure 14 c-d. Areas in between the bubbles are ash free. 3D animations of the chars are available via the links in the web version of the article [174] (Paper III). Comparing the compositions of the accumulated ash at the surface there was a trend for less potassium and more calcium in the ash at the higher temperature, even though not statistically validated due to uncertainties probably caused by variations between pellets. For the samples combusted at 700°C, there was a trend for less potassium at higher conversion. This might be the result of reactions at 1,000°C reaching equilibrium more rapidly, favored by a larger fraction of the ash being melted.

Inside the char particle, accumulation of denser ash compounds were found on surfaces surrounding the cavities. These places with accumulated ash contained more silicon and less calcium than the ash that surrounded the char. During the conversion process, an increased proportion of accumulated ash around the cavities and more accumulated ash closer to the surface were identified. Silicon rich beads were also present in the chars, sometimes partly dissolved in the melted ash. These particles were probably Phytoliths (silica), which originate from the plant material of the wheat straw [175, 176]. Small bubbles developed at the cavities closer to the surface in the later part of conversion for the 1,000°C char. In addition, the composition of the melt around the cavities had similar compositions to the bubbles in the later part of the char conversion at 1,000°C.

The wheat straw pellets were also combusted in a domestic pellet boiler (Paper IV). The melted residue ash formed silicate slag; a hard lump was formed in the burner when it cooled down (Figure 15). The residue ash was analyzed using SEM-EDS, and the results indicated similar relative compositions of the main ash-forming elements as that of the residue left after combustion in the single pellet furnace.

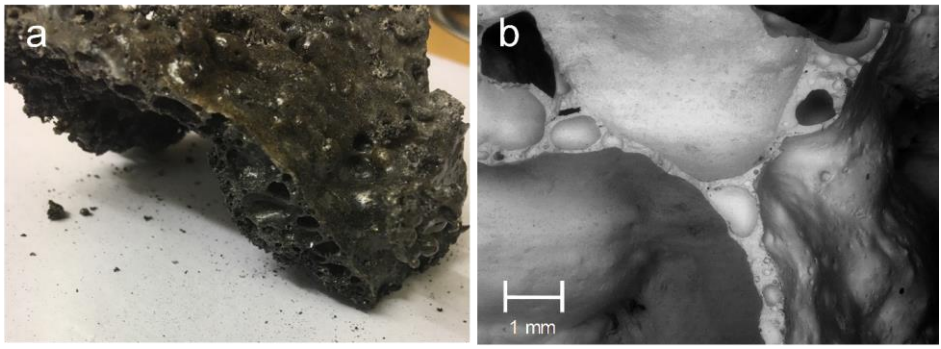

Figure 15. a) Slag residue of wheat straw collected after combustion in the domestic pellet boiler. b) SEM micrograph cross-section of a piece of the slag residue. Adapted from Paper IV.

A phase diagram can be used to study the melting behavior of the residual ash; the slagging tendencies of the wheat straw ash with given composition are displayed using the ternary system of K_2O – CaO – SiO_2 in Figure 16. Fuels, pellets and chars and residual ashes are included. Here, MgO behavior was approximated to be similar to CaO, and MgO was added to CaO. Another assumption is that contribution by phosphorus was left out. The phase diagram with liquidus isotherms can be useful to indicate the composition and temperature at which high slagging tendencies can be expected. The liquidus isotherms in Figure 16 show that the composition of the ash and char from WS 125 μm in the phase diagram is linked to a eutectic point located at about 750°C. This is in agreement with the results of ash residue which is only loosely sintered at the lower gasification temperatures (700-750°C) in Paper II, while the ash residue was completely melted at higher temperatures. In Papers III-IV the actual pellet temperature for WS700 chars was about 900°C, and in this case, the ash residue also appears to have been melted to some extent.

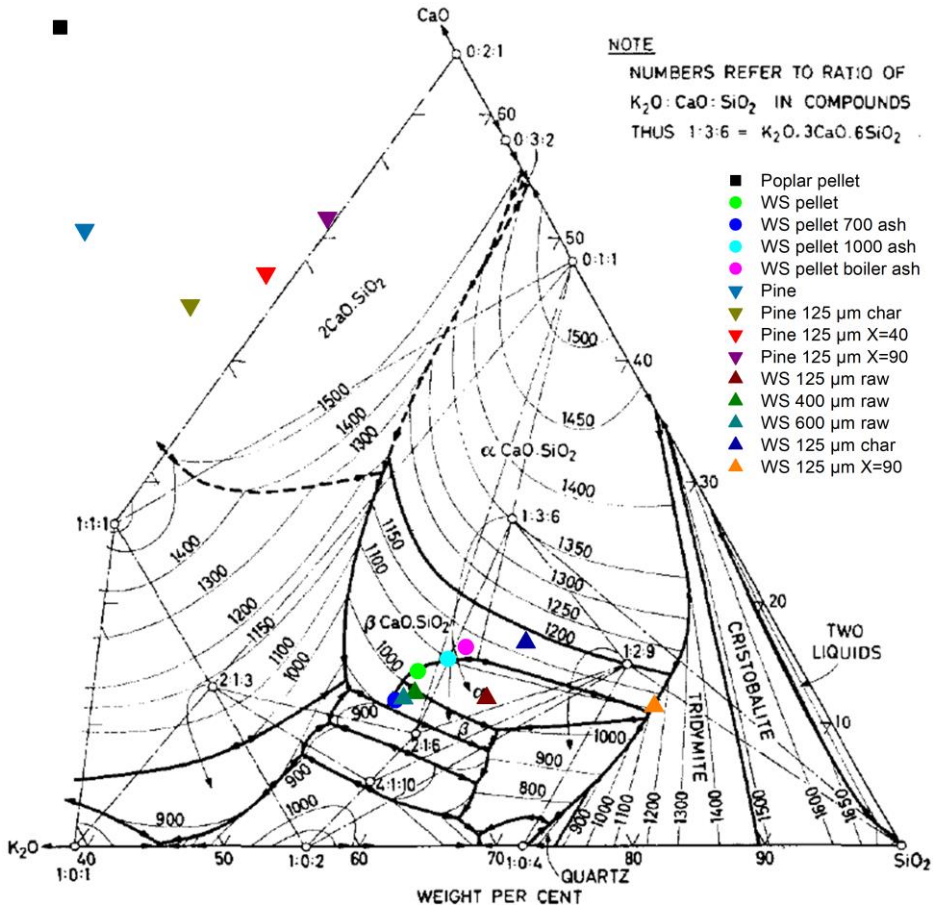

Figure 16. Ternary compositional diagram (wt%). The raw fuel/pellets data came from standard fuel analysis and the char and ash data are results from the EDS analyses. The data were normalized to the content of SiO_2, K_2O and CaO (+MgO). The phase diagram was adapted, with permission, from Fig. 23 in Silicate Melt Systems, Physics and Chemistry of the Earth, Roedder [177]. Copyright (1959) Published by Elsevier Ltd.

The release of potassium found at both devolatilization and char gasification from the wheat straw in Paper II was not seen for the combustion of wheat straw pellets; instead, most of the potassium remained in the silicate ash. The relative composition of potassium, calcium and silicon for the wheat straw particles and the pellet are similar (presented in the ternary system of K_2O – CaO – SiO_2 in Figure 16). Probably, the reason for the difference in release behavior of potassium between the particles and the pellets was related to the conditions in the respective experimental setup; in Paper II, the wheat straw particles were first rapidly devolatilized in a DTF at 900-1,100°C, quench cooled, and then later reheated and gasified in TGA (at 850°C in this case). During devolatilization in

the DTF, potassium might rapidly undergo primarily ash transformation reactions, while the time and contact was too limited for silicon to capture the potassium and form silicates. Rapidly produced gas phase potassium compounds are in agreement with results found by e.g. Qu et al. [178] and Wagner et al. [130]. During heating and gasification of the chars in the TGA, potassium continued to be released, possibly partially due to competition with calcium [19, 21, 97, 98]. The potassium could than leave the silicate, primarily as KOH. It could also be related to particle size and form, and thus the probability that potassium is caught by silicon during char conversion.

The woody fuels used in this study do not fit in to this part of the ternary diagram. They are located to the left, closer to calcium in the upper corner. In particular, the poplar wood used is close to calcium, and the tendency to form silicate-based slag is low. However, at least for the pinewood, there may be some sites in the ash with locally higher silicon concentrations, and silicate slag could be formed.

The slagging tendencies of a fuel depends on both the fraction of melt and its viscosity, i.e. the potential stickiness of the melt, and these vary depending on the fuel content of e.g. potassium, calcium and silicon [96]. Viscosity estimation was performed in Paper IV using the viscosity toolbox in FactSage. The viscosity was calculated for the composition of the accumulated ash surrounding the char and the ash residue after full conversion and assumed that everything was melt. Since relative compositions of the ash-forming elements were quite similar for the samples at the different temperatures, the differences in viscosity for the melt corresponding to WS700 chars and WS1000 chars are mainly due to the strong temperature dependence. The estimated viscosities were higher for WS700 compared to WS1000, which was in agreement with the observations using SEM and micro-tomographic scans, where the WS700 ash appeared rather solid, while the lower viscosity of the WS1000 allowed for the formation of liquid and bubbles.

4.2.2 Ca-rich carbonate and oxide forming fuels

Calcium- and potassium-rich, woody biomass was used in Paper II (pine stemwood) and Papers III and V (poplar pellets). Pine stemwood was rich not only in calcium and potassium but also magnesium, followed by silicon, phosphorus and sulfur. In contrast, poplar wood was rich in phosphorus, followed by magnesium and only had low amounts of silicon and sulfur.

In Paper II, when high-heating rate char originating from pine stemwood particles was gasified in TGA at different temperatures, the result after full conversion was a calcium-rich low density, porous ash layer. Formation of this powdery ash layer was seen at an earlier stage of conversion (at X_{wt}=0.4 and

X_{wt}=0.9 in Figure 17a and b, respectively) using interrupted TGA gasification experiments at 850°C, analyzed with SEM-EDS. Some areas of partial melting can be seen in the later stage of conversion (Figure 17b). EDS spot analysis indicated locally higher silicon concentrations inducing a silicate melt. Potassium was to a large extent released during devolatilization in the DTF, and the potassium content continued to decrease during ash formation.

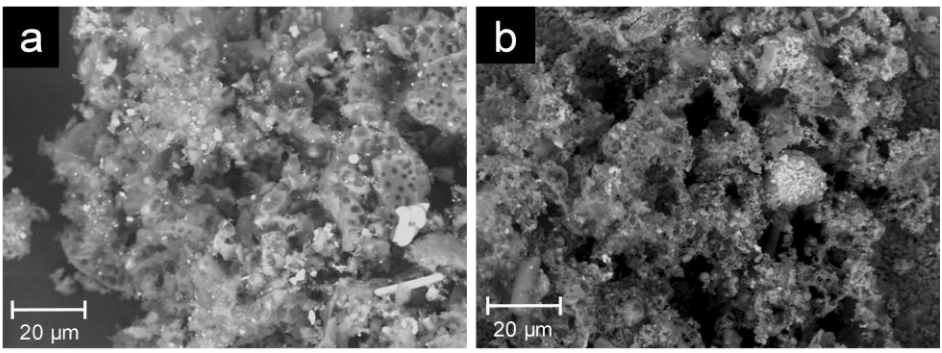

Figure 17. SEM micrographs of solid residues from TGA gasification at 850°C of pine wood char powder, interrupted at conversion of a) X_{wt} = 0.40 and b) X_{wt}=0.90. Adapted with permission from Effects of Pyrolysis Conditions and Ash Formation on Gasification Rates of Biomass Char, Strandberg et al. [173] (paper II). Copyright (2017) American Chemical Society.

According to thermodynamic calculations, potassium, calcium and magnesium should be present as carbonates or oxides in addition to silicates. The non-melted appearance of the remaining ash supports these assumptions. The mixed K-Ca-carbonates are stable up to approximately 900°C under the CO_2 purged conditions in the TGA. If carbonates are formed, and if their catalytic effect is correctly understood, the increase in conversion rate in the later part of char conversion can be explained by the increased contact between char and carbonates. At higher temperatures, normalized conversion rates decrease, which might be caused by chemical phase transformations resulting in deactivation or loss of catalytic compounds. The stability of carbonates is dependent on the local partial pressures of CO_2 and H_2O. This requires further consideration in process applications in which a syngas loaded gas atmosphere is very different to that of the analysis.

The Poplar pellets used in Paper III and Paper V contained a lot of calcium and potassium. The total ash content was much higher compared to the pine stemwood used in Paper II, and relative compositions showed more phosphorus and less silicon for the poplar fuel. The ash layer formed during combustion was a light grey, low density, porous powder. SEM-EDS analysis showed that the poplar ash residue contains high amounts of calcium with smaller fractions of

potassium, magnesium, and phosphorus. The poplar pellets and the charred poplar pellets from combustion experiments at 1,000°C were also scanned using X-ray micro-tomography (Paper III). Figure 18 visualizes 3D reconstruction of poplar char with color mapped using X-ray absorption. Unlike wheat straw, which clearly revealed the formation of ash melts during conversion, the char from poplar pellets did not show any accumulation of the ash layer on the surfaces from the tomographic images until the very end of the conversion, probably due to the low density of the ash in combination with the small quantity. In addition, for the char in the later part of conversion, as shown in Figure 18 b, quenched at 91 $_{wt}$% of char conversion, a great part of the outer ash layer fell off before the micro-tomographic scan. Results from micro-tomography (Figure 18) show regions with particles of higher density, but without any obvious evidence of mobility or melting during conversion, except for accumulation on the surface due to the disappearance of the char as the conversion proceeds. These regions of higher density correspond well to pieces of poplar bark, also seen as dark regions in the fuel pellets that could contain large calcium oxalate crystals. The immobility was as expected, due to the fact that calcium is considered to be non-volatile. Transport of the more volatile potassium was not detected, and it is obvious that more detailed chemical analyses were needed for this fuel.

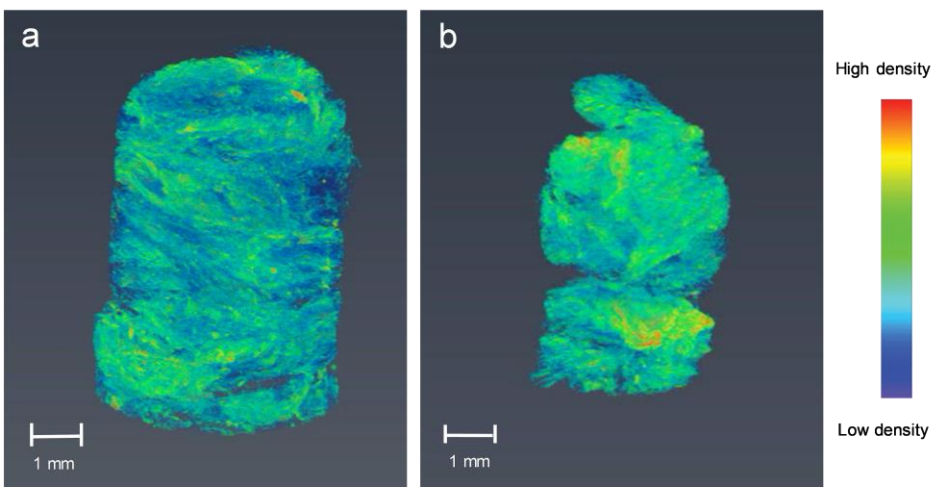

Figure 18. 3D reconstructions with color mapped by X-ray absorption, (density) from 2.0 μ to 4.6 μ, of a) Poplar 1000 at X_{wt} = 0.40, b) Poplar 1000 at X_{wt} = 0.91. Adapted in parts from Strandberg et al. [174] (Paper III). Animation of the figure is available via the links in the web version of the article.

In the study presented in Paper V, powder XRD and SEM-EDS were used for more detailed chemical and structural analysis of the same poplar pellets. In this case, the pellets were combusted in the single pellet furnace in air with a furnace temperature of 700°C, and also in an atmosphere of 20 $_{vol}$% CO_2 together with air, at furnace temperatures of 600-1,000°C. CO_2 in the supply gas was used with the aim of approaching the combustion conditions in a fuel bed, with the potential for carbonate formation. Without this addition, the atmosphere surrounding the single pellet during conversion would not reach relevant CO_2 partial pressures for carbonate stability. The partial pressure of H_2O was not varied in this study, even though it is also known to be important for carbonate stability. Experiments performed in air with no added CO_2 to see the effects of efficiently diluting/flushing the CO_2 from the reactions were in agreement with the hypothesis of less stable carbonate formation. After full conversion at a furnace temperature of 700°C almost no carbonates remained. Interestingly, carbonates were present earlier during the char conversion phase (at 75% of the time of the char conversion), indicating the conditions where the actual ash forming reactions take place, with sufficiently high local pCO_2 generated by the combustion to stabilize carbonates.

Figure 19 presents the relative composition of the main ash-forming elements from the EDS analysis of the samples. As expected, less potassium was retained in the char/ashes at higher temperatures. A weak trend of potassium content decreasing with conversion was found particularly at the higher temperatures.

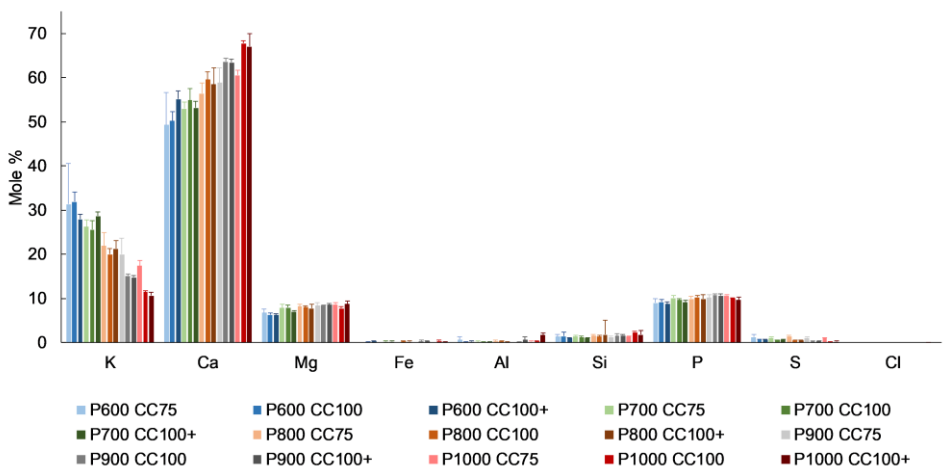

Figure 19. Relative compositions of the main ash-forming elements according to EDS analysis after combustion of poplar wood pellets at different temperatures in an atmosphere of 20 vol% CO_2 in air, quenched at different points. CC75 is sample quenched at 75 % of the time for char conversion, CC100 is at full conversion, and CC100+ is full conversion plus 30 seconds. Adapted from Paper V.

XRD quantification was not accurately quantitative for a complete mass balance, mainly missing potassium and in some case also phosphorus, which might be a result of a limitation in the method with disagreements due to possible amorphous phases (XRD only identifies crystalline phases) or poorly crystallized/very small crystals in small amounts. However, despite this, it gives a useful indication of the trends.

In agreement with thermodynamic modelling, carbonates were common in the samples from lower temperatures; $CaCO_3$ (calcite), $K_2Ca_2(CO_3)_3$, and $K_2Ca(CO_3)_2$ (fairchildite) were identified using XRD. In addition, carbonate apatite, $Ca_{9.9}(PO_4)_6(CO_3)_{0.9}$ were found. Hydroxyapatite is commonly found in combustion products [21], but the XRD pattern obtain in these experiments better match with carbonate apatite. The presence of carbonates and some other crystalline compounds in the sample are shown in Figure 20. At higher temperature, calcium oxide (CaO) was the dominant phase. Generally, carbonates were more common at lower temperature, and their presence decreased as the temperature increased. Thermodynamic equilibrium calculations for conditions corresponding to those in the experiments indicate that the solid carbonates $CaCO_3$ and $K_2Ca_2(CO_3)_3$ are stable up to around 750°C; subsequently, first $CaCO_3$ decomposes to CaO, and at a slightly higher temperature $K_2Ca_2(CO_3)_3$ decomposes to CaO and $K_2Ca(CO_3)_2$. At about 800°C a melt consisting of K_2CO_3 and $CaCO_3$ is formed. Just before 900°C (depending on pCO_2, pH_2O, and dilution), this carbonate is calcined into CaO(s) and KOH(g). XRD analysis showed that the fraction of potassium retained at high temperatures was in the form of $KCaPO_4$.

The degree of conversion was found to have an effect on Ca-carbonates which appeared to decrease in quantity from samples quenched for 75% of the time for char conversion to full conversion, and for higher temperatures they appeared to decompose close to full conversion. The temperature in the pellet was higher than the furnace temperature during char conversion, but when the char reached full conversion, the temperature of the sample decreased to the same temperature as the furnace [134]. Together with the 20% CO_2 in the reactor atmosphere, this can lead to reformation of the Ca-carbonates at temperatures up to 900°C; this could be the explanation for the increase seen for some of the carbonates found in samples which remained in the furnace for 30 seconds after full conversion.

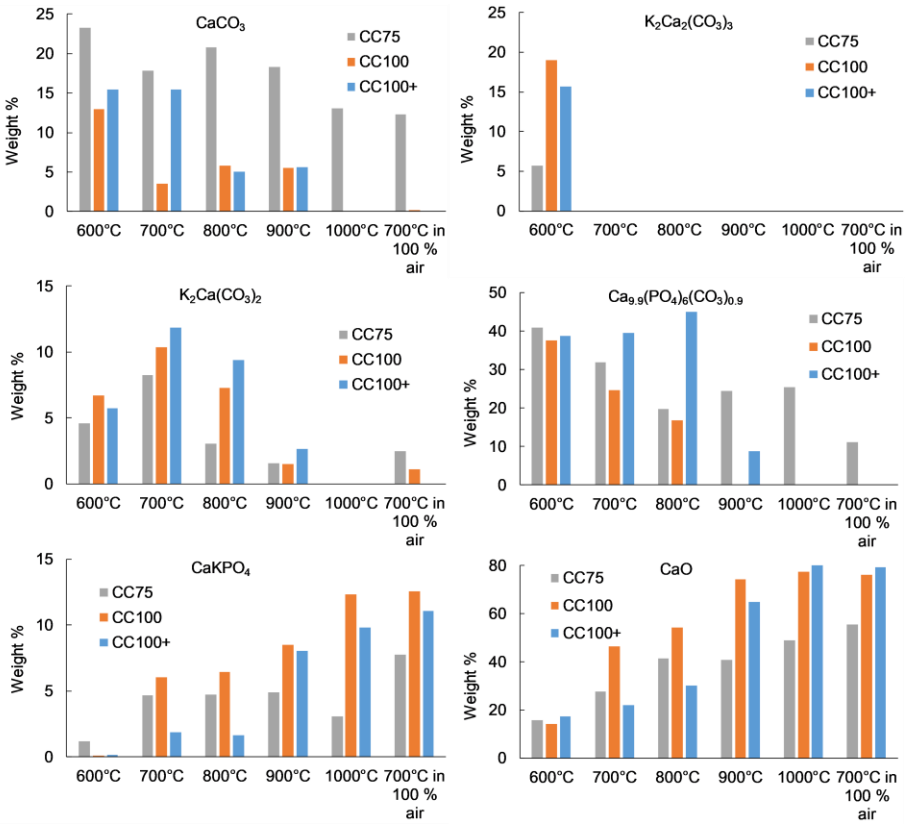

Figure 20. Some of the crystalline compounds in weight percent of total crystalline phases found in the samples during the XRD analysis. CC75 is sample quenched at 75% of the time for char conversion, CC100 is at full conversion, and CC100+ is full conversion plus 30 seconds. Adapted from Paper V.

Figure 21 shows the morphology of the residual ashes from poplar pellets after combustion in an atmosphere of 20 $_{vol}$% CO_2 in air at different temperatures. Indications of melting were seen in some parts of the samples, but there were no clear differences between the temperatures. Some differences between temperatures were found and in Figure 21 close-ups of calcium rich particles look solid and stable at low temperatures (a), while similar particles seems to have become porous, but without falling apart, at higher temperatures (b-c). This is in good agreement with the expected transformation of calcium oxalate upon heating, including carbonate formation and possible calcination.

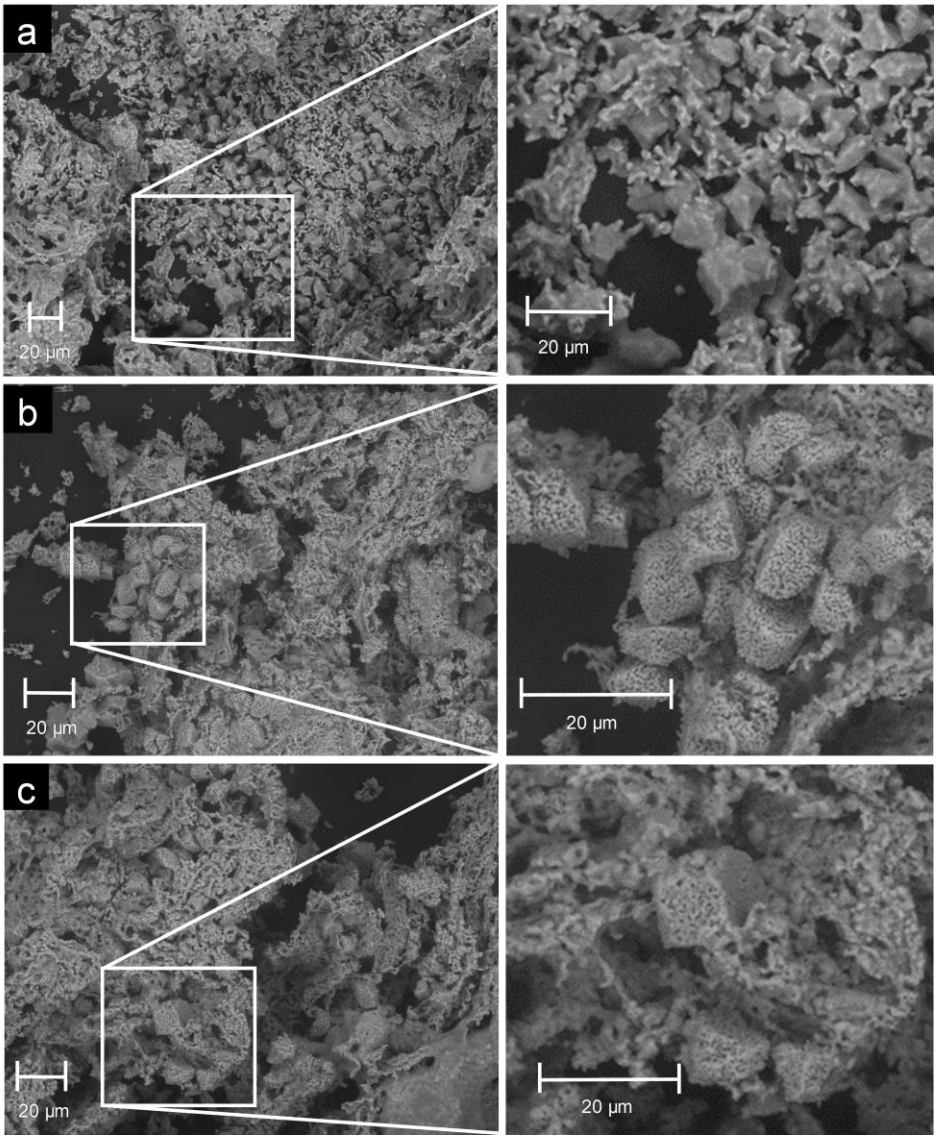

Figure 21. Backscattered electron pictures of ash residue from poplar pellet at full conversion after combustion in an atmosphere of 20 $_{vol}$% CO_2 and 80 $_{vol}$% air at a furnace temperature of a) 600°C, b) 800°C and c) 1,000°C. Adapted from Paper V.

5 Conclusions

The present thesis presents new conversion-based explanations and detailed insights into changes in structure and ash properties during conversion of lignocellulosic biomass.

In Paper I, it was concluded that combined TGA and multivariate data analysis could be useful for predictions of compositional information and fuel properties of thermally pre-treated wood. The multivariate approach performed better compared to a conventional method, with an error of prediction of 2.7%. The method can be useful as a characterization tool in future studies involving small samples.

Paper II presents the results from a study investigating the reactivity of high heating rate chars from pine stemwood and wheat straw at different original particle sizes. Reactivity dependence on original particle size was found only for the smallest pine chars, which had higher intrinsic char gasification rates. Furthermore, we concluded that the char conversion rate was influenced by the ash composition, not only for the active char sites, but also through ash layer formation. For pine wood, increased rates with conversion were found, which are supported by the established understanding of "catalytic effects" of potassium compounds. A decreased effect with increasing temperature might be explained by the chemical phase transformations of carbonates. Chars from pine wood formed a porous, calcium-rich ash layer, with no sign of limiting the conversion rate. Wheat straw, on the other hand, was found to be physically inhibited by a Si/K/Ca-rich melt. The melted ash formed a layer that encapsulated the remaining char in the later stages of conversion, probably limiting the contact between the char and gasification agent. This highlighted that kinetic conversion studies on fuels with low temperature melting ash might be problematic, since the encapsulation forms a diffusion barrier, which prevents the reaction taking place in the targeted kinetically controlled regime, at least at the later stage of conversion.

In Paper III, we demonstrated that single pellet combustion at high temperature (1,000°C) produced numerous cracks and internal cavities in the char during the later part of devolatilization, and that they continued to form during at least the first part of the char oxidation phase. Quantification of shrinking during conversion and the development of internal cavities was performed using data from X-ray micro-tomography of chars from poplar wood and wheat straw pellets.

As expected, large variations between the ash layer properties were found between the different fuels. Poplar wood pellets formed a porous, calcium-rich ash layer, whereas for wheat straw pellets, the silicate melt formed bubbles on the surface at high combustion temperature. These bubbles increased in both number and size as the conversion proceeded but without totally encapsulating the char and blocking the gas transport. One explanation why wheat straw pellets demonstrate only a slightly longer total conversion time compared to poplar wood (12% longer) might be that the surface of the wheat straw pellets was only partially covered by the melted ash. However, the observed effect on conversion rate could not be totally distinguished from those of other differences between the fuels.

Results from this study show good opportunities for further use of micro-tomography to acquire detailed insights into changes in structure and ash properties for biomass fuel, chars and ash samples. This study also provides new knowledge from single pellet conversion that can be useful for improving or developing more accurate and flexible fuel particle conversion models.

In Paper IV, the experiments with wheat straw pellets combusted at 1,000°C (Paper III) were complemented with 700°C experiments. At lower temperature in the furnace (700°C), the wheat straw ash formed more of a rigid net structure as the conversion proceeded, with apparently lower melt fraction. The difference in composition of the ash was small, but at higher temperature there were indications of relatively less potassium and more calcium accumulation in the ash. In addition, there was a trend for potassium loss and calcium accumulation in the ash with increasing conversion, most valid for the 700°C experiments, and was explained by the 1,000°C samples reaching equilibrium more rapidly. Combustion experiments in a domestic boiler showed evidence of extensive melting, and the resulting slag consisted of numerous bubbles with similar relative composition to that of the residue after combustion in the single pellet furnace.

Limiting char burnout by ash layers that encapsulate the char seen in Paper II, was not found to any greater extent at the single pellet level (Papers III-IV), nor in the experiment in a small domestic boiler (Paper IV). However, ash layers that block gas transport and limit char burnout during combustion might still be a problem with other fuels, or in larger grate-fired units with potential for more ash accumulation on the char bed surface, and where the temperature and gas distribution might be different.

Powder X-ray diffraction (XRD) and scanning electron microscopy (SEM) used to analyze combustion residues from poplar pellets (Paper V), provided

temperature and conversion profiles for concentrations of ash-forming elements and crystalline phases. The carbonates $CaCO_3$ (calcite), $K_2Ca_2(CO_3)_3$, $K_2Ca(CO_3)_2$ (fairchildite) and $Ca_{9.9}(PO_4)_6(CO_3)_{0.9}$ (apatite A (CO_3-bearing)) were identified using XRD at lower temperatures and the presence of carbonates decreased when the temperature increased. At higher temperatures, CaO (lime) was the dominant phase. The experimental results were in good agreement with thermodynamic calculations. This provided new insights in the ash formation and transformations taking place, and in the actual conditions in and on the fuel where the ash is formed.

6 Future work

Fuel particle conversion models have the potential to assist in the optimization of fuel conversion processes. However, for use with pelletized biomasses, these models need to be adapted if accurate mechanistic models on particle level is desired, since most models today are developed for uncompressed biomass particles. This study indicates that the development of cracks and internal cavities during pellet conversion is very different from that previously described for uncompressed biomass particles. One implication is that an accurate description of pore development and density change during conversion must also take these observations into account. A useful and accurate fuel particle conversion model must also include more detailed information on the impact of ash formation. It is also necessary to study the development of cracks and internal cavities and the impact of ash formation during pellet conversion at lower temperatures.

X-ray micro-tomography has shown to be very useful in providing detailed insights into changes in structure and ash properties during conversion. This technique could be used to examine other types of biomasses, different types of particles, and different conversion technologies. It also offers the potential to generate more information from the samples, such as identification of high-density ashes and studying their morphology. In-situ scanning of thermal conversion processes could also provide new useful results.

In paper V, we report the results from a study on the presence of carbonates and oxides at different combustion temperatures for poplar wood pellets. At higher temperatures, we found only oxides. One interesting remaining question is whether the carbonates formed during an early stage of combustion when the surrounding temperature is high at all times, and later decomposed, or if they never formed due to the high heating rate and local conditions. Also the practical implications, i.e. how ash transformations are affected by the actual conditions in a boiler, remains to be evaluated, as well characterizations of resulting operational problems.

Acknowledgement

First of all, Markus Broström, thank you for making this journey possible, it has been very instructive and a great time! I'm very glad I've had you as my supervisor. I have learned a lot from you, and thanks for always have a minute to spare for all the questions I have come up with. Thanks for all the support!

I will also like to thank my co-supervisors, Christoffer Boman and Rainer Backman. Christoffer, thanks for the discussions around single pellet combustion and your "last minute work" with my paper V is much appreciated. Rainer, your knowledge and experience are valuable, thanks for rewarding discussions.

To all my great colleagues at TEC-lab and former ETPC, both past and present, thank you for being there and making this time fun and rewarding. Eleonora Borén, a special thanks to you for nice coffee breaks and crafting nights, and thanks for all your help around the dissertation and with the cover illustration. Nils Skoglund and Jonathan Fagerström, your enthusiasm and engaging discussions aroused my interest for research, and helped me with my decision to search away from my previous job, seven years ago. Keep going like that!
Thanks to all my co-authors:

Per Holmgren and David R. Wagner, thanks for the useful discussions around calculations, results, limitations and other things in life as well.

Roger Molinder and Henrik Wiinikka for welcoming us to your drop-tube furnace in Piteå, and with the help around the experimental campaign.

Kentaro Umeki, it was very instructive and valuable to have you in discussions around conversion rates and reactivity, and it was nice to work with you.

Torbjörn Lestander, Mikael Thyrel, Rainer Backman, Markus Broström, and Nils Skoglund; thank you for making the application and for letting me join on the exciting trip to the synchrotron at ALS in Berkeley. I learned a lot from all of you and together we made it to a memorable trip. An extra thanks to Mikael for the power of the computer and the time you spent on the image analysis.

Markus Carlborg thank you for introducing me to the interesting analysis with XRD, the rewarding discussions, and your patient with all my XRD related questions.

I will also thank the facilities and technical support (Cheng Choo Lee) of the Umeå Core Facility for Electron Microscopy (UCEM) at the Chemical Biological Centre (KBC), Umeå University.

This research used the resources of the Advanced Light Source (ALS), at Lawrence Berkeley National Laboratory, Berkeley, California, which is a DOE Office of Science User Facility under contract no. DE-AC02-05CH11231 (ALS-08232 T.A.L). Access to ALS Beamline 8.3.2 is much appreciated, and we thank Research Scientist Dr Dula Parkinson for invaluable assistance with the analyses at ALS. Johannes Koestel at the X-ray facility of the Department of Soil and Environment, Swedish University of Agricultural Sciences, Sweden, is greatly acknowledged for the X-ray micro-tomography analysis of the WS700 chars that gave an extra dimension to paper IV. I would also like to acknowledge the support of Bio4Energy, a strategic research environment appointed by the Swedish government.

Till min familj: Mina föräldrar och syskon, tack för att ni har funnits där och stöttat och uppmuntrat, utan att ställa för stora krav. Stort tack för all hjälpen under de här åren, med barnvakt, både hemma och på resor, och uppbackning och hjälp i övrigt. Till mina barn, Tuva och Sofie, tack för all glädje och kärlek ni kommer med. Jag hoppas att ni får har kvar mycket av er nyfikenhet, glädje och viljestyrka genom hela livet. Sist, men inte minst, Martin, tack för att du finns här med mig. Jag uppskattar verkligen att du stöttat och fixat så att jag kunnat lägga mycket tid nu i slutet på att bli klar med detta arbete. Det har även varit mycket värdefullt med dina kommentarer, frågor och uppmuntran. Jag älskar er!

References

[1] CO2 Emissions From Fuel Combustion Highlights 2017, in, International Energy Agency, in IEA statistics, OECD, Paris, 2017.
[2] IPCC, Climate Change 2013: The Physical Science Basis. Contribution of Working Group I to the Fifth Assessment Report of the Intergovernmental Panel on Climate Change, in, [Stocker, T.F., D. Qin, G.-K. Plattner, M. Tignor, S.K. Allen, J. Boschung, A. Nauels, Y. Xia, V. Bex and P.M. Midgley (eds.)]. Cambridge University Press, Cambridge, United Kingdom and New York, NY, USA, 1535 pp., 2013.
[3] J. Rockström, W. Steffen, K. Noone, Å. Persson, F.S. Chapin, E. Lambin, T.M. Lenton, M. Scheffer, C. Folke, H.J. Schellnhuber, B. Nykvist, C.A. de Wit, T. Hughes, S. van der Leeuw, H. Rodhe, S. Sörlin, P.K. Snyder, R. Costanza, U. Svedin, M. Falkenmark, L. Karlberg, R.W. Corell, V.J. Fabry, J. Hansen, B. Walker, D. Liverman, K. Richardson, P. Crutzen, J. Foley, Planetary Boundaries, Exploring the Safe Operating Space for Humanity, Ecology and Society, 14 (2009).
[4] W. Steffen, K. Richardson, J. Rockström, S.E. Cornell, I. Fetzer, E.M. Bennett, R. Biggs, S.R. Carpenter, W. de Vries, C.A. de Wit, C. Folke, D. Gerten, J. Heinke, G.M. Mace, L.M. Persson, V. Ramanathan, B. Reyers, S. Sörlin, Planetary boundaries: Guiding human development on a changing planet, Science, 347 (2015).
[5] United Nations Framework Convension on Climate Change. (2016) in, The paris agreement, URL: http://unfccc.int/paris_agreement/items/9485.php, 04/30/2018
[6] M. Balat, G. Ayar, Biomass Energy in the World, Use of Biomass and Potential Trends, Energy Sources, 27 (2005) 931-940.
[7] L. Wang, J. Sandquist, G. Varhegyi, B. Matas Güell, CO2 Gasification of Chars Prepared from Wood and Forest Residue: A Kinetic Study, Energy & Fuels, (2013).
[8] L.P. Koh, J. Ghazoul, Biofuels, biodiversity, and people: Understanding the conflicts and finding opportunities, Biological Conservation, 141 (2008) 2450-2460.
[9] S.V. Vassilev, D. Baxter, L.K. Andersen, C.G. Vassileva, T.J. Morgan, An overview of the organic and inorganic phase composition of biomass, Fuel, 94 (2012) 1-33.
[10] M. Hoogwijk, A. Faaij, R. van den Broek, G. Berndes, D. Gielen, W. Turkenburg, Exploration of the ranges of the global potential of biomass for energy, Biomass and Bioenergy, 25 (2003) 119-133.
[11] G. Tao, T.A. Lestander, P. Geladi, S. Xiong, Biomass properties in association with plant species and assortments I: a synthesis based on literature data of energy properties, Renewable and Sustainable Energy Reviews, 16 (2012) 3481-3506.
[12] A. Monti, N. Di Virgilio, G. Venturi, Mineral composition and ash content of six major energy crops, Biomass and Bioenergy, 32 (2008) 216-223.
[13] S.V. Vassilev, D. Baxter, L.K. Andersen, C.G. Vassileva, An overview of the chemical composition of biomass, Fuel, 89 (2010) 913-933.

[14] J. Werkelin, B.J. Skrifvars, M. Hupa, Ash-forming elements in four Scandinavian wood species. Part 1: Summer harvest, Biomass & Bioenergy, 29 (2005) 451-466.
[15] G. Tao, P. Geladi, T.A. Lestander, S. Xiong, Biomass properties in association with plant species and assortments. II: A synthesis based on literature data for ash elements, Renewable and Sustainable Energy Reviews, 16 (2012) 3507-3522.
[16] J. Werkelin, D. Lindberg, D. Boström, B.J. Skrifvars, M. Hupa, Ash-forming elements in four Scandinavian wood species part 3: Combustion of five spruce samples, Biomass & Bioenergy, 35 (2011) 725-733.
[17] F.J. Frandsen, Utilizing biomass and waste for power production—a decade of contributing to the understanding, interpretation and analysis of deposits and corrosion products, Fuel, 84 (2005) 1277-1294.
[18] L.L. Baxter, T.R. Miles, T.R. Miles, B.M. Jenkins, T. Milne, D. Dayton, R.W. Bryers, L.L. Oden, The behavior of inorganic material in biomass-fired power boilers: field and laboratory experiences, Fuel Processing Technology, 54 (1998) 47-78.
[19] C. Gilbe, M. Öhman, E. Lindström, D. Boström, R. Backman, R. Samuelsson, J. Burvall, Slagging characteristics during residential combustion of biomass pellets, Energy & Fuels, 22 (2008) 3536-3543.
[20] S.V. Vassilev, C.G. Vassileva, Y.-C. Song, W.-Y. Li, J. Feng, Ash contents and ash-forming elements of biomass and their significance for solid biofuel combustion, Fuel, 208 (2017) 377-409.
[21] D. Boström, N. Skoglund, A. Grimm, C. Boman, M. Öhman, M. Broström, R. Backman, Ash Transformation Chemistry during Combustion of Biomass, Energy & Fuels, 26 (2012) 85-93.
[22] C. Di Blasi, Combustion and gasification rates of lignocellulosic chars, Progress in Energy and Combustion Science, 35 (2009) 121-140.
[23] H. Thunman, B. Leckner, F. Niklasson, F. Johnsson, Combustion of wood particles—a particle model for Eulerian calculations, Combustion and Flame, 129 (2002) 30-46.
[24] M.A. Gómez, J. Porteiro, D. Patiño, J.L. Míguez, Fast-solving thermally thick model of biomass particles embedded in a CFD code for the simulation of fixed-bed burners, Energy Conversion and Management, 105 (2015) 30-44.
[25] H. Ström, H. Thunman, A computationally efficient particle submodel for CFD-simulations of fixed-bed conversion, Applied Energy, 112 (2013) 808-817.
[26] K. Umeki, S.-a. Roh, T.-j. Min, T. Namioka, K. Yoshikawa, A simple expression for the apparent reaction rate of large wood char gasification with steam, Bioresource Technology, 101 (2010) 4187-4192.
[27] Y.B. Yang, V.N. Sharifi, J. Swithenbank, L. Ma, L.I. Darvell, J.M. Jones, M. Pourkashanian, A. Williams, Combustion of a single particle of biomass, Energy & Fuels, 22 (2007) 306-316.
[28] A. Gómez-Barea, B. Leckner, Modeling of biomass gasification in fluidized bed, Progress in Energy and Combustion Science, 36 (2010) 444-509.
[29] Y. Haseli, J.A. van Oijen, L.P.H. de Goey, A detailed one-dimensional model of combustion of a woody biomass particle, Bioresource Technology, 102 (2011) 9772-9782.
[30] R. Mehrabian, S. Zahirovic, R. Scharler, I. Obernberger, S. Kleditzsch, S. Wirtz, V. Scherer, H. Lu, L.L. Baxter, A CFD model for thermal conversion of

thermally thick biomass particles, Fuel Processing Technology, 95 (2012) 96-108.
[31] H. Ström, H. Thunman, CFD simulations of biofuel bed conversion: A submodel for the drying and devolatilization of thermally thick wood particles, Combustion and Flame, 160 (2013) 417-431.
[32] J. Porteiro, E. Granada, J. Collazo, D. Patino, J. Morán, A model for the combustion of large particles of densified wood, Energy and Fuels, 21 (2007) 3151-3159.
[33] J. Porteiro, J. Collazo, D. Patino, E. Granada, J.C. Moran Gonzalez, J.L.s. Míguez, Numerical modeling of a biomass pellet domestic boiler, Energy & Fuels, 23 (2009) 1067-1075.
[34] A.K. Biswas, K. Umeki, Simplification of devolatilization models for thermally-thick particles: Differences between wood logs and pellets, Chemical Engineering Journal, 274 (2015) 181-191.
[35] D. Nutalapati, R. Gupta, B. Moghtaderi, T.F. Wall, Assessing slagging and fouling during biomass combustion: A thermodynamic approach allowing for alkali/ash reactions, Fuel Processing Technology, 88 (2007) 1044-1052.
[36] H. Ström, F. Niklasson, A. Hjörnhede, S. Hermansson, Experimental and Numerical Investigations of Ash Behaviour in Fixed-Bed Combustion of Woody Biomass Pellets, in: Proceedings of the Nordic Flame Days 2017, Stockholm, Swede, 2017.
[37] H. Fatehi, Numerical Simulation of Combustion and Gasification of Biomass Particles, 2014.
[38] A.C. O'SULLIVAN, Cellulose: the structure slowly unravels, Cellulose, 4 (1997) 173-207.
[39] H.V. Scheller, P. Ulvskov, Hemicelluloses, Annu Rev Plant Biol, 61 (2010) 263-289.
[40] K. Werner, L. Pommer, M. Broström, Thermal decomposition of hemicelluloses, Journal of Analytical and Applied Pyrolysis, 110 (2014) 130-137.
[41] M.M. Campbell, R.R. Sederoff, Variation in Lignin Content and Composition (Mechanisms of Control and Implications for the Genetic Improvement of Plants), Plant Physiology, 110 (1996) 3-13.
[42] E. Meszaros, E. Jakab, G. Varhegyi, P. Szepesvary, B. Marosvolgyi, Comparative study of the thermal behavior of wood and bark of young shoots obtained from an energy plantation, Journal of Analytical and Applied Pyrolysis, 72 (2004) 317-328.
[43] B. Sander, Properties of Danish biofuels and the requirements for power production, Biomass and Bioenergy, 12 (1997) 177-183.
[44] A. Nordin, Chemical elemental characteristics of biomass fuels, Biomass and Bioenergy, 6 (1994) 339-347.
[45] I. Obernberger, F. Biedermann, W. Widmann, R. Riedl, Concentrations of inorganic elements in biomass fuels and recovery in the different ash fractions, Biomass and Bioenergy, 12 (1997) 211-224.
[46] M. Zevenhoven, P. Yrjas, B.-J. Skrifvars, M. Hupa, Characterization of Ash-Forming Matter in Various Solid Fuels by Selective Leaching and Its Implications for Fluidized-Bed Combustion, Energy & Fuels, 26 (2012) 6366-6386.

[47] S.V. Vassilev, D. Baxter, L.K. Andersen, C.G. Vassileva, An overview of the composition and application of biomass ash. Part 1. Phase–mineral and chemical composition and classification, Fuel, 105 (2013) 40-76.
[48] M. Zevenhoven-Onderwater, Ash-forming matter in biomass fuels, Åbo Akademi Åbo/Turku, Finland, 2001.
[49] V. Doshi, H.B. Vuthaluru, R. Korbee, J.H.A. Kiel, Development of a modeling approach to predict ash formation during co-firing of coal and biomass, Fuel Processing Technology, 90 (2009) 1148-1156.
[50] W. Stelte, A.R. Sanadi, L. Shang, J.K. Holm, J. Ahrenfeldt, U.B. Henriksen, Recent developments in biomass pelletization–A review, BioResources, 7 (2012) 4451-4490.
[51] J. Werther, M. Saenger, E.U. Hartge, T. Ogada, Z. Siagi, Combustion of agricultural residues, Progress in Energy and Combustion Science, 26 (2000) 1-27.
[52] D. Thraen, D. Peetz, K. Schaubach, T. Mai-Moulin, H. Junginger, P. Lamers, L. Visser, Global wood pellet industry and trade study 2017, Paris, France: IEA Bioenergy) p, 243 (2017).
[53] D. Bergström, S. Israelsson, M. Öhman, S.-A. Dahlqvist, R. Gref, C. Boman, I. Wästerlund, Effects of raw material particle size distribution on the characteristics of Scots pine sawdust fuel pellets, Fuel Processing Technology, 89 (2008) 1324-1329.
[54] R. Samuelsson, S. Larsson, M. Thyrel, T. A. Lestander, Moisture content and storage time influences the binding mechanisms in biofuel pellets, 2012.
[55] R. Samuelsson, M. Thyrel, M. Sjöström, T. A. Lestander, Effect of biomaterial characteristics on pelletizing properties and biofuel pellet quality, 2009.
[56] C. Rhen, M. Ohman, R. Gref, I. Wasterlund, Effect of raw material composition in woody biomass pellets on combustion characteristics, Biomass and Bioenergy, 31 (2007) 66-72.
[57] A.K. Biswas, M. Rudolfsson, M. Broström, K. Umeki, Effect of pelletizing conditions on combustion behaviour of single wood pellet, Applied Energy, 119 (2014) 79-84.
[58] A. Nordin, L. Pommer, M. Nordwaeger, I. Olofsson, Biomass conversion through torrefaction, in: Technologies for converting biomass to useful energy: Combustion, Gasification, Pyrolysis, Torrefaction and Fermentation, CRC Press, 2013, pp. 217-244.
[59] J.J. Chew, V. Doshi, Recent advances in biomass pretreatment – Torrefaction fundamentals and technology, Renewable and Sustainable Energy Reviews, 15 (2011) 4212-4222.
[60] M.J.C. van der Stelt, H. Gerhauser, J.H.A. Kiel, K.J. Ptasinski, Biomass upgrading by torrefaction for the production of biofuels: A review, Biomass and Bioenergy, 35 (2011) 3748-3762.
[61] M. Strandberg, I. Olofsson, L. Pommer, S. Wiklund-Lindström, K. Åberg, A. Nordin, Effects of temperature and residence time on continuous torrefaction of spruce wood, Fuel Processing Technology, 134 (2015) 387-398.
[62] W.-H. Chen, P.-C. Kuo, A study on torrefaction of various biomass materials and its impact on lignocellulosic structure simulated by a thermogravimetry, Energy, 35 (2010) 2580-2586.

[63] B. Arias, C. Pevida, J. Fermoso, M.G. Plaza, F. Rubiera, J.J. Pis, Influence of torrefaction on the grindability and reactivity of woody biomass, Fuel Processing Technology, 89 (2008) 169-175.
[64] C.D. Blasi, Physico-chemical processes occurring inside a degrading two-dimensional anisotropic porous medium, International Journal of Heat and Mass Transfer, 41 (1998) 4139-4150.
[65] D. Semino, L. Tognotti, Modelling and sensitivity analysis of pyrolysis of biomass particle in a fluidised bed, Computers & Chemical Engineering, 22, Supplement 1 (1998) S699-S702.
[66] C. Di Blasi, Modeling chemical and physical processes of wood and biomass pyrolysis, Progress in Energy and Combustion Science, 34 (2008) 47-90.
[67] L. Lin, E. Gustafsson, M. Strand, Aerosol-based method for investigating biomass char reactivity at high temperatures, Combustion and Flame, 158 (2011) 1426-1437.
[68] J. Fermoso, C. Stevanov, B. Moghtaderi, B. Arias, C. Pevida, M.G. Plaza, F. Rubiera, J.J. Pis, High-pressure gasification reactivity of biomass chars produced at different temperatures, Journal of Analytical and Applied Pyrolysis, 85 (2009) 287-293.
[69] E. Cetin, B. Moghtaderi, R. Gupta, T.F. Wall, Influence of pyrolysis conditions on the structure and gasification reactivity of biomass chars, Fuel, 83 (2004) 2139-2150.
[70] R. Zanzi, K. Sjöström, E. Björnbom, Rapid high-temperature pyrolysis of biomass in a free-fall reactor, Fuel, 75 (1996) 545-550.
[71] C. Di Blasi, Kinetic and heat transfer control in the slow and flash pyrolysis of solids, Industrial & Engineering Chemistry Research, 35 (1996) 37-46.
[72] L. Wei, S. Xu, L. Zhang, H. Zhang, C. Liu, H. Zhu, S. Liu, Characteristics of fast pyrolysis of biomass in a free fall reactor, Fuel Processing Technology, 87 (2006) 863-871.
[73] H.-C. Kung, A mathematical model of wood pyrolysis, Combustion and Flame, 18 (1972) 185-195.
[74] P.S. Maa, R.C. Bailie, Influence of particle sizes and environmental conditions on high temperature pyrolysis of cellulosic material—I (Theoretical), Combustion Science and Technology, 7 (1973) 257-269.
[75] D.L. Pyle, C.A. Zaror, Heat transfer and kinetics in the low temperature pyrolysis of solids, Chemical Engineering Science, 39 (1984) 147-158.
[76] P. Holmgren, D.R. Wagner, A. Strandberg, R. Molinder, H. Wiinikka, K. Umeki, M. Broström, Size, shape, and density changes of biomass particles during rapid devolatilization, Fuel, 206 (2017) 342-351.
[77] A. Trubetskaya, P.A. Jensen, A.D. Jensen, A.D. Garcia Llamas, K. Umeki, P. Glarborg, Effect of fast pyrolysis conditions on biomass solid residues at high temperatures, Fuel Processing Technology, 143 (2016) 118-129.
[78] M. Sreekanth, A.K. Kolar, B. Leckner, A semi-analytical model to predict primary fragmentation of wood in a bubbling fluidized bed combustor, Journal of Analytical and Applied Pyrolysis, 83 (2008) 88-100.
[79] I. Smith, The combustion rates of coal chars: a review, in: Symposium (International) on Combustion, Elsevier, 1982, pp. 1045-1065.
[80] C. Guizani, F.J. Escudero Sanz, S. Salvador, The gasification reactivity of high-heating-rate chars in single and mixed atmospheres of H2O and CO2, Fuel, 108 (2013) 812-823.

[81] H. Jameel, D.R. Keshwani, S. Carter, T. Treasure, J. Cheng, Thermochemical conversion of biomass to power and fuels, Biomass to renewable energy processes, 10 (2010) 437-487.
[82] J.J. Hernández, G. Aranda-Almansa, A. Bula, Gasification of biomass wastes in an entrained flow gasifier: Effect of the particle size and the residence time, Fuel Processing Technology, 91 (2010) 681-692.
[83] I.I. Ahmed, A.K. Gupta, Particle size, porosity and temperature effects on char conversion, Applied Energy, 88 (2011) 4667-4677.
[84] C. Higman, M. Van Der Burgt, Gasification, Second edition ed., 2008.
[85] N.M. Laurendeau, Heterogeneous kinetics of coal char gasification and combustion, Progress in Energy and Combustion Science, 4 (1978) 221-270.
[86] R.H. Hurt, Structure, properties, and reactivity of solid fuels, Symposium (International) on Combustion, 27 (1998) 2887-2904.
[87] P.L. Walker, F. Rusinko, L.G. Austin, Gas Reactions of Carbon, in: D.D. Eley, P.W. Selwood, P.B. Weisz (Eds.) Advances in Catalysis, Academic Press, 1959, pp. 133-221.
[88] M. Rossberg, E. Wicke, Transportvorgänge und Oberflächenreaktionen bei der Verbrennung graphitischen Kohlenstoffs, Chemie Ingenieur Technik, 28 (1956) 181-189.
[89] E.W. Thiele, Relation between catalytic activity and size of particle, Industrial & Engineering Chemistry, 31 (1939) 916-920.
[90] P. Ollero, A. Serrera, R. Arjona, S. Alcantarilla, Diffusional effects in TGA gasification experiments for kinetic determination, Fuel, 81 (2002) 1989-2000.
[91] B. Nowak, O. Karlström, P. Backman, A. Brink, M. Zevenhoven, S. Voglsam, F. Winter, M. Hupa, Mass transfer limitation in thermogravimetry of biomass gasification, Journal of Thermal Analysis and Calorimetry, 111 (2013) 183-192.
[92] A. Gómez-Barea, P. Ollero, C. Fernández-Baco, Diffusional Effects in CO2 Gasification Experiments with Single Biomass Char Particles. 1. Experimental Investigation, Energy & Fuels, 20 (2006) 2202-2210.
[93] J.H. Flynn, Thermal analysis kinetics-problems, pitfalls and how to deal with them, Journal of Thermal Analysis, 34 (1988) 367-381.
[94] A. Moilanen, J. Vepsalainen, E. Kurkela, J. Konttinen, Gasification reactivity of large biomass pieces, Science in thermal and chemical biomass conversion, (2006) 509-517.
[95] P. Thy, B.M. Jenkins, C.E. Lesher, High-Temperature Melting Behavior of Urban Wood Fuel Ash, Energy & Fuels, 13 (1999) 839-850.
[96] I.-L. Näzelius, J. Fagerström, C. Boman, D. Boström, M. Öhman, Slagging in Fixed-Bed Combustion of Phosphorus-Poor Biomass: Critical Ash-Forming Processes and Compositions, Energy & Fuels, 29 (2015) 894-908.
[97] P. Thy, C.E. Lesher, B.M. Jenkins, Experimental determination of high-temperature elemental losses from biomass slag, Fuel, 79 (2000) 693-700.
[98] N. Skoglund, Ash chemistry and fuel design focusing on combustion of phosphorus-rich biomass, in, Umeå universitet, Umeå, 2014, pp. 50.
[99] P.A. Jensen, F.J. Frandsen, K. Dam-Johansen, B. Sander, Experimental investigation of the transformation. and release to gas phase of potassium and chlorine during straw pyrolysis, Energy & Fuels, 14 (2000) 1280-1285.
[100] J.N. Knudsen, P.A. Jensen, K. Dam-Johansen, Transformation and Release to the Gas Phase of Cl, K, and S during Combustion of Annual Biomass, Energy & Fuels, 18 (2004) 1385-1399.

[101] M. Zevenhoven-Onderwater, R. Backman, B.-J. Skrifvars, M. Hupa, The ash chemistry in fluidised bed gasification of biomass fuels. Part I: predicting the chemistry of melting ashes and ash–bed material interaction, Fuel, 80 (2001) 1489-1502.
[102] I.-L. Näzelius, D. Boström, A. Rebbling, C. Boman, M. Öhman, Fuel Indices for Estimation of Slagging of Phosphorus-Poor Biomass in Fixed Bed Combustion, Energy & Fuels, 31 (2017) 904-915.
[103] P.A. Tchoffor, F. Moradian, A. Pettersson, K.O. Davidsson, H. Thunman, Influence of Fuel Ash Characteristics on the Release of Potassium, Chlorine, and Sulfur from Biomass Fuels under Steam-Fluidized Bed Gasification Conditions, Energy & Fuels, 30 (2016) 10435-10442.
[104] J.N. Knudsen, P.A. Jensen, W. Lin, F.J. Frandsen, K. Dam-Johansen, Sulfur Transformations during Thermal Conversion of Herbaceous Biomass, Energy & Fuels, 18 (2004) 810-819.
[105] B. Olanders, B.-M. Steenari, Characterization of ashes from wood and straw, Biomass and Bioenergy, 8 (1995) 105-115.
[106] P. Thy, B.M. Jenkins, S. Grundvig, R. Shiraki, C.E. Lesher, High temperature elemental losses and mineralogical changes in common biomass ashes, Fuel, 85 (2006) 783-795.
[107] M.K. Misra, K.W. Ragland, A.J. Baker, Wood ash composition as a function of furnace temperature, Biomass and Bioenergy, 4 (1993) 103-116.
[108] Y. Huang, X. Yin, C. Wu, C. Wang, J. Xie, Z. Zhou, L. Ma, H. Li, Effects of metal catalysts on CO2 gasification reactivity of biomass char, Biotechnology Advances, 27 (2009) 568-572.
[109] J. Kramb, N. DeMartini, M. Perander, A. Moilanen, J. Konttinen, Modeling of the catalytic effects of potassium and calcium on spruce wood gasification in CO 2, Fuel Processing Technology, 148 (2016) 50-59.
[110] J.M. Jones, L.I. Darvell, T.G. Bridgeman, M. Pourkashanian, A. Williams, An investigation of the thermal and catalytic behaviour of potassium in biomass combustion, Proceedings of the Combustion Institute, 31 (2007) 1955-1963.
[111] F. Suárez-García, A. Martínez-Alonso, M. Fernández Llorente, J.M.D. Tascón, Inorganic matter characterization in vegetable biomass feedstocks, Fuel, 81 (2002) 1161-1169.
[112] M. Perander, N. DeMartini, A. Brink, J. Kramb, O. Karlström, J. Hemming, A. Moilanen, J. Konttinen, M. Hupa, Catalytic effect of Ca and K on CO2 gasification of spruce wood char, Fuel, 150 (2015) 464-472.
[113] K. Kirtania, J. Axelsson, L. Matsakas, P. Christakopoulos, K. Umeki, E. Furusjö, Kinetic study of catalytic gasification of wood char impregnated with different alkali salts, Energy, 118 (2017) 1055-1065.
[114] J.A. Moulijn, M.B. Cerfontain, F. Kapteijn, Mechanism of the potassium catalysed gasification of carbon in CO2, Fuel, 63 (1984) 1043-1047.
[115] D.A. Sams, F. Shadman, Mechanism of potassium-catalyzed carbon/CO2 reaction, AIChE Journal, 32 (1986) 1132-1137.
[116] B.J. Wood, R.H. Fleming, H. Wise, Reactive intermediate in the alkali-carbonate-catalysed gasification of coal char, Fuel, 63 (1984) 1600-1603.
[117] C.A. Mims, J.K. Pabst, Role of surface salt complexes in alkali-catalysed carbon gasification, Fuel, 62 (1983) 176-179.

[118] K. Umeki, A. Moilanen, A. Gómez-Barea, J. Konttinen, A model of biomass char gasification describing the change in catalytic activity of ash, Chemical Engineering Journal, 207–208 (2012) 616-624.
[119] C. Dupont, T. Nocquet, J.A. Da Costa Jr, C. Verne-Tournon, Kinetic modelling of steam gasification of various woody biomass chars: Influence of inorganic elements, Bioresource Technology, 102 (2011) 9743-9748.
[120] C. Hognon, C. Dupont, M. Grateau, F. Delrue, Comparison of steam gasification reactivity of algal and lignocellulosic biomass: Influence of inorganic elements, Bioresource Technology, 164 (2014) 347-353.
[121] M.P. Kannan, G.N. Richards, Gasification of biomass chars in carbon dioxide: dependence of gasification rate on the indigenous metal content, Fuel, 69 (1990) 747-753.
[122] Z. Bouraoui, M. Jeguirim, C. Guizani, L. Limousy, C. Dupont, R. Gadiou, Thermogravimetric study on the influence of structural, textural and chemical properties of biomass chars on CO2 gasification reactivity, Energy, 88 (2015) 703-710.
[123] C. Chen, T. Kojima, Single char particle combustion at moderate temperature: effects of ash, Fuel Processing Technology, 47 (1996) 215-232.
[124] Y. Niu, C.R. Shaddix, A sophisticated model to predict ash inhibition during combustion of pulverized char particles, Proceedings of the Combustion Institute, 35 (2015) 561-569.
[125] H. Liu, H. Zhu, M. Kaneko, S. Kato, T. Kojima, High-temperature gasification reactivity with steam of coal chars derived under various pyrolysis conditions in a fluidized bed, Energy & Fuels, 24 (2009) 68-75.
[126] A. Zolin, A. Jensen, P.A. Jensen, F. Frandsen, K. Dam-Johansen, The influence of inorganic materials on the thermal deactivation of fuel chars, Energy & Fuels, 15 (2001) 1110-1122.
[127] C. Branca, A. Iannace, C. Di Blasi, Devolatilization and combustion kinetics of Quercus cerris bark, Energy & Fuels, 21 (2007) 1078-1084.
[128] M. Strandberg, From torrefaction to gasification : Pilot scale studies for upgrading of biomass, in: Applied Physics and Electronics, Umeå University, 2015.
[129] R. Molinder, H. Wiinikka, Feeding small biomass particles at low rates, Powder Technology, 269 (2015) 240-246.
[130] D.R. Wagner, P. Holmgren, A. Strandberg, H. Wiinikka, R. Molinder, M. Broström, Fate of Inorganic Species during Biomass Devolatilization in a Drop Tube Furnace, in: Impacts of Fuel Quality on Power Production, 2014.
[131] A.M.C. Janse, H.G. de Jonge, W. Prins, W.P.M. van Swaaij, Combustion kinetics of char obtained by flash pyrolysis of pine wood, Industrial & Engineering Chemistry Research, 37 (1998) 3909-3918.
[132] A. Moilanen, K. Saviharju, Gasification Reactivities of Biomass Fuels in Pressurised Conditions and Product Gas Mixtures, in: A.V. Bridgwater, D.G.B. Boocock (Eds.) Developments in Thermochemical Biomass Conversion: Volume 1 / Volume 2, Springer Netherlands, Dordrecht, 1997, pp. 828-837.
[133] K. Yip, M. Xu, C.-Z. Li, S.P. Jiang, H. Wu, Biochar as a Fuel: 3. Mechanistic Understanding on Biochar Thermal Annealing at Mild Temperatures and Its Effect on Biochar Reactivity, Energy & Fuels, 25 (2011) 406-414.

[134] J. Fagerström, E. Steinvall, D. Boström, C. Boman, Alkali transformation during single pellet combustion of soft wood and wheat straw, Fuel Processing Technology, 143 (2016) 204-212.
[135] J. Fagerström, I.-L. Näzelius, C. Gilbe, D. Boström, M. Öhman, C. Boman, Influence of peat ash composition on particle emissions and slag formation in biomass grate co-combustion, Energy & Fuels, 28 (2014) 3403-3411.
[136] ASTM, Standard Test Method for Compositional Analysis by Thermogravimetry, in: E1131 – 08, 2008.
[137] J.I. Goldstein, C.E. Lyman, D.E. Newbury, E. Lifshin, P. Echlin, L. Sawyer, D.C. Joy, J.R. Michael, Scanning electron microscopy and X-ray microanalysis, Kluwer Academic/Plenum Publishers,, New York, 2003.
[138] R.F. Egerton, Physical principles of electron microscopy, Springer, 2005.
[139] R.C. Gonzalez, R.E. Woods, Digital Image Processing, New Jersy: Pearson Education, in, Inc, 2008.
[140] A. MacDowell, D. Parkinson, A. Haboub, E. Schaible, J. Nasiatka, C. Yee, J. Jameson, J. Ajo-Franklin, C. Brodersen, A. McElrone, X-ray micro-tomography at the Advanced Light Source, in: Proc. SPIE, 2012, pp. 850618.
[141] A.J. McElrone, B. Choat, D.Y. Parkinson, A.A. MacDowell, C.R. Brodersen, Using High Resolution Computed Tomography to Visualize the Three Dimensional Structure and Function of Plant Vasculature, Journal of Visualized Experiments : JoVE, (2013) 50162.
[142] D. Wildenschild, C. Vaz, M. Rivers, D. Rikard, B. Christensen, Using X-ray computed tomography in hydrology: systems, resolutions, and limitations, Journal of Hydrology, 267 (2002) 285-297.
[143] A.R. West, Basic solid state chemistry, John Wiley & Sons Inc, 1988.
[144] W.H. Bragg, Bragg, W. L., The reflection of X-rays by crystals, Proceedings of the Royal Society of London. Series A, 88 (1913) 428-438.
[145] Powder Diffraction File, PDF-2, International Center for Diffraction Data (ICDD): Newtowne Square, PA, (2004).
[146] Inorganic crystal structure database, ICSD, in, National Institute of Standards and Technology, Fachinformationzentrum Karlsruhe: Karlsruhe, Germany.
[147] L. Eriksson, E. Johansson, N. Kettaneh-Wold, J. Trygg, C. Wikström, S. Wold, Multi- and Megavariate Data Analysis : Part I: Basic Principles and Applications, 2:nd edition ed., Umetrics AB, 2006.
[148] J.A. Persson, E. Johansson, C. Albano, Quantitative thermogravimetry of peat. A multivariate approach, Analytical Chemistry, 58 (1986) 1173-1178.
[149] G.E. Acquah, B.K. Via, O.O. Fasina, S. Adhikari, N. Billor, L.G. Eckhardt, Chemometric modeling of thermogravimetric data for the compositional analysis of forest biomass, PLOS ONE, 12 (2017) e0172999.
[150] K. Bergner, C. Albano, Thermal analysis of peat, Analytical Chemistry, 65 (1993) 204-208.
[151] T.A. Lestander, M. Rudolfsson, L. Pommer, A. Nordin, NIR provides excellent predictions of properties of biocoal from torrefaction and pyrolysis of biomass, Green Chemistry, 16 (2014) 4906-4913.
[152] C.-L. So, T.L. Eberhardt, FTIR-based models for assessment of mass yield and biofuel properties of torrefied wood, Wood Science and Technology, 52 (2018) 209-227.

[153] S. Lande, S. Riel, O. Høibø, A. Schneider, M. Schneider, H. Schneider, Development of chemometric models based on near infrared spectroscopy and thermogravimetric analysis for predicting the treatment level of furfurylated Scots pine, Wood Science and Technology, 44 189-203.
[154] S. Wold, M. Sjöström, L. Eriksson, PLS-regression: a basic tool of chemometrics, Chemometrics and Intelligent Laboratory Systems, 58 (2001) 109-130.
[155] L. Eriksson, J. Trygg, S. Wold, A chemometrics toolbox based on projections and latent variables, Journal of Chemometrics, 28 (2014) 332-346.
[156] S. Wold, H. Martens, H. Wold, The multivariate calibration problem in chemistry solved by the PLS method, in: Matrix pencils, Springer, 1983, pp. 286-293.
[157] P. Geladi, B.R. Kowalski, Partial least-squares regression: a tutorial, Anal Chim Acta, 185 (1986) 1-17.
[158] H. Stenlund, Improving interpretation by orthogonal variation : Multivariate analysis of spectroscopic data, in, Kemiska institutionen, Umeå universitet, Umeå, 2011, pp. 62.
[159] T. Chai, R.R. Draxler, Root mean square error (RMSE) or mean absolute error (MAE)? – Arguments against avoiding RMSE in the literature, Geosci. Model Dev., 7 (2014) 1247-1250.
[160] B. Galindo-Prieto, Novel variable influence on projection (VIP) methods in OPLS, O2PLS, and OnPLS models for single- and multi-block variable selection : VIPOPLS, VIPO2PLS, and MB-VIOP methods, in, Umeå University, Umeå, 2017, pp. 103.
[161] C. Bale, P. Chartrand, S. Degterov, G. Eriksson, K. Hack, R.B. Mahfoud, J. Melançon, A. Pelton, S. Petersen, FactSage thermochemical software and databases, Calphad - Computer Coupling of Phase Diagrams and Thermochemistry, 26 (2002) 189-228.
[162] C.W. Bale, E. Bélisle, P. Chartrand, S.A. Decterov, G. Eriksson, K. Hack, I.H. Jung, Y.B. Kang, J. Melançon, A.D. Pelton, C. Robelin, S. Petersen, FactSage thermochemical software and databases — recent developments, Calphad - Computer Coupling of Phase Diagrams and Thermochemistry, 33 (2009) 295-311.
[163] D. Lindberg, R. Backman, P. Chartrand, M. Hupa, Towards a comprehensive thermodynamic database for ash-forming elements in biomass and waste combustion—Current situation and future developments, Fuel Processing Technology, 105 (2013) 129-141.
[164] W.-Y. Kim, A.D. Pelton, S.A. Decterov, A model to calculate the viscosity of silicate melts: Part III: Modification for melts containing alkali oxides, International Journal of Materials Research, 103 (2012) 313-328.
[165] A.N. Grundy, I.-H. Jung, A.D. Pelton, S.A. Decterov, A model to calculate the viscosity of silicate melts: Part II: The NaO0. 5–MgO–CaO–AlO1. 5–SiO2 system, International Journal of Materials Research, 99 (2008) 1195-1209.
[166] A.N. Grundy, H. Liu, I.-H. Jung, S.A. Decterov, A.D. Pelton, A model to calculate the viscosity of silicate melts: Part I: Viscosity of binary SiO2# x2013; MeO x systems (Me= Na, K, Ca, Mg, Al), International Journal of Materials Research, 99 (2008) 1185-1194.

[167] M. Broström, A. Nordin, L. Pommer, C. Branca, C. Di Blasi, Influence of torrefaction on the devolatilization and oxidation kinetics of wood, Journal of Analytical and Applied Pyrolysis, 96 (2012) 100-109.
[168] A. Strandberg, P. Holmgren, M. Broström, Predicting fuel properties of biomass using thermogravimetry and multivariate data analysis, Fuel Processing Technology, 156 (2017) 107-112.
[169] H. Watanabe, X-ray Computed Tomography Visualization of the Woody Char Intraparticle Pore Structure and Its Role on Anisotropic Evolution during Char Gasification, Energy & Fuels, (2018).
[170] T. Pattanotai, H. Watanabe, K. Okazaki, Gasification characteristic of large wood chars with anisotropic structure, Fuel, 117 (2014) 331-339.
[171] H. Ström, S. Sasic, H. Thunman, Challenges and Opportunities in the Eulerian Approach to Numerical Simulations of Fixed-bed Combustion of Biomass, Procedia Engineering, 102 (2015) 1573-1582.
[172] D.W. McKee, Mechanisms of the alkali metal catalysed gasification of carbon, Fuel, 62 (1983) 170-175.
[173] A. Strandberg, P. Holmgren, D.R. Wagner, R. Molinder, H. Wiinikka, K. Umeki, M. Broström, Effects of Pyrolysis Conditions and Ash Formation on Gasification Rates of Biomass Char, Energy & Fuels, 31 (2017) 6507-6514.
[174] A. Strandberg, M. Thyrel, N. Skoglund, T.A. Lestander, M. Broström, R. Backman, Biomass pellet combustion: Cavities and ash formation characterized by synchrotron X-ray micro-tomography, Fuel Processing Technology, 176 (2018) 211-220.
[175] H. Chen, F. Wang, C. Zhang, Y. Shi, G. Jin, S. Yuan, Preparation of nano-silica materials: The concept from wheat straw, Journal of Non-Crystalline Solids, 356 (2010) 2781-2785.
[176] F. Guntzer, C. Keller, J.-D. Meunier, Benefits of plant silicon for crops: a review, Agronomy for Sustainable Development, 32 (2012) 201-213.
[177] E. Roedder, Silicate melt systems, Physics and Chemistry of the Earth, 3 (1959) 224-297.
[178] Z. Qu, P. Holmgren, N. Skoglund, D.R. Wagner, M. Broström, F.M. Schmidt, Distribution of temperature, H2O and atomic potassium during entrained flow biomass combustion – Coupling in situ TDLAS with modeling approaches and ash chemistry, Combustion and Flame, 188 (2018) 488-497.